Journal of Urban and Environmental Engineering

E-ISSN: 1982-3932

celso@ct.ufpb.br

Universidade Federal da Paraíba

Brasil

Márquez, Adriana M.; Guevara-Pérez, Edilberto

COMPARATIVE ANALYSIS OF EROSION MODELING TECHNIQUES IN A BASIN OF VENEZUELA

Journal of Urban and Environmental Engineering, vol. 4, núm. 2, julio-diciembre, 2010, pp. 81-104

Universidade Federal da Paraíba

Paraíba, Brasil

Journal of Urban and Environmental Engineering, v.4, n.2, p.81-104
ISSN 1982-3932
doi: 10.4090/juee.2010.v4n2.081104

Journal of Urban and Environmental Engineering
www.journal-uee.org

COMPARATIVE ANALYSIS OF EROSION MODELING TECHNIQUES IN A BASIN OF VENEZUELA

Adriana M. Márquez* and Edilberto Guevara-Pérez
Centre of Environmental and Hydrologic Research, Carabobo University, Venezuela

Received 20 May 2010; received in revised form 20 October 2010; accepted 16 December 2010

Abstract: This paper investigates a comparative analysis of erosion modeling techniques based on deterministic models, both empirically-based and process-based models. The empirical modeling is based on statistical and artificial intelligence techniques. In the first, two types of statistical regression model structures are investigated, a linear multiple regression model structure and a nonlinear multiple regression model structure. In the second, tools such as artificial neural networks (ANN) and fuzzy inference system (FIS) are used. The physical process-based modeling involves the calibration, validation and testing of the models components: WEPP, EUROSEM and CIHAM-UC. The input and output variables of models were collected during rainy and dry (irrigation) seasons in Chirgua river basin, Venezuela for two years (2008–2009). Ninety-seven rainfall storms and 300 irrigation events were measured. Satisfactory fit was found in the techniques investigated, R^2 close to 0.7.

Keywords: Sediments; hydrological models; soil erosion model; regression model; hydrology; runoff; artificial neural networks; fuzzy inference systems

* Correspondence to: Adriana Márquez. Telefax: 0058-414-4165856.
E-mail: ammarquez@uc.edu.ve

INTRODUCTION

The conventional techniques of erosion modeling are empirically and process-based. The empirical models include the Universal Soil Loss Equation (USLE) (Wischmeier & Smith, 1958), and its latter developments, Revised Soil Loss Equation (RUSLE) and Modified Universal Soil Loss Equation (MUSLE) (Renard *et al.*, 1997a, 1997b). The process-based models are represented, e.g., by the WEPP (Water Erosion Prediction Project) (Flanagan *et al.*, 2001), DWEPP (Dynamic Water Erosion Prediction Project) (Bulygina *et al.*, 2007) and EUROSEM (European Soil Erosion Model) (Morgan *et al.*, 1998). There have been a large number of studies to calibrate and validate the runoff and erosion components of process-based models (e.g., Flanagan *et al.*, 1995; Klik *et al.*, 1995; Savabi *et al.*, 1996; Zhang *et al.*, 1996; Nearing *et al.*, 1998; Zeleke, 1999; Ranieri *et al.*, 1999; Santoro *et al.*, 2002; Bulygin *et al.*, 2002; Laflen *et al.*, 2004; Silva *et al.*, 2007; Santos *et al.*, 2003). Many erosion models require a large amount of data for calibration and validation as well as high performance, meaning, the complex algorithms, execution times that eventually cause problems, and a programming language necessary to minimize the time compute. Additionally, the ANN and FIS have been proposed as efficient tools for modeling and hydrology forecasting (e.g., Bishop, 1994; Jain & Ormsbee, 2002; Panigrahi & Mujundar, 2000). In this work, process-based models, statistical regression, ANN's and FIS's are used to model the furrow erosion process.

It is generally assumed that furrow erosion processes are similar to rill erosion processes that occur under rainfall. There are similarities in the processes, but there are also differences in the conditions (Trout & Niebling, 1993). Most rainfall erosion occurs during a few highly erosive events, while furrow erosion occurs at low-to-moderate rates during several irrigations with controlled water application. Most irrigation furrows are on slopes of less than 3%, while most rill erosion research is carried out on slopes greater than 3%. However, in spite of the controlled inflows and relatively low slopes, in some areas with highly erodible soils, there is significant furrow irrigation causing erosion damage (Koluvec *et al.*, 1993; Trout, 1999). The present study had two main objectives: (1) calibrate, validate and test models for the estimation of furrow erosion processes and (2) compare experimentally observed furrow erosion processes with simulated results by different methods.

MODEL DESCRIPTION

Water Erosion Prediction Project

WEPP model was developed by the United States Service (USDA-ARS). This model is based on steady-state equation assuming a uniform downslope overland flow; therefore, variables are expressed on a total width or total area basis (Foster & Meyer, 1975; Foster, 1982; Foster & Lane, 1987; Foster, 1990). WEPP distinguishes erosion processes involved in interrill and rill erosion. The basic relationship is given by:

$$\frac{\partial(CA)}{\partial t} + \frac{\partial(CQ)}{\partial x} = S \tag{1}$$

where C is the concentration of sediment in the flow (kg/m^3), A the cross-sectional area of flow (m^2), Q the flow discharge (m^3/s), t the time (s), x the distance downslope (m), the term $\partial(CQ)/\partial x$ the rate of change of sediment with the distance, $\partial(CA)/\partial t$ the storage rate of sediment within the flow depth, S the source/sink term for sediment (kg/s/m^2) is given by:

$$S = D_I + D_R \tag{2}$$

By assuming quasi-steady sediment movement, **Eq. (1)** is reduced to:

$$\frac{\partial(CQ)}{\partial x} = D_I + D_R \tag{3}$$

$$D_R = \begin{cases} D_c\left(1 - \dfrac{CQ}{wT_c}\right), & \mathrm{CQ} \le \mathrm{wT_c} \\ \dfrac{0.5V_s}{Q}\left(wT_c - CQ\right), & \mathrm{CQ} \ge \mathrm{wT_c} \end{cases} \tag{4}$$

where D_I is the interrill sediment delivery to the rill (kg/s/m^2), D_R the flow erosion rate (kg/s/m^2), T_c the flow transport capacity in the rill (kg/s/m), w the rill width, V_s the particle fall velocity (m/s), Q the flow discharge (m^3/s), and D_c the flow soil detachment capacity (kg/s/m^2) is computed as:

$$D_c = \begin{cases} K_r(\tau - \tau_c), & \tau \ge \tau_c \\ 0, & \tau \le \tau_c \end{cases} \tag{5}$$

$$\tau = \rho_W g S R \tag{6}$$

where K_r is the rill erodibility (s/m), τ the flow shear stress acting on the soil (Pa), τ_c the critical shear stress (Pa), ρ_w the water density (kg/m^3), g the acceleration due to gravity (m/s^2), S slope (m/m), R hydraulic radius (m). Rills are assumed to be rectangular with widths that depend on flow rate.

The simplified form of the equation of Yalin, (1963) to estimate the sediment transport capacity has been adapted by Foster & Meyer, (1975) as:

where T_c is the sediment transport capacity, a and b are coefficients obtained by empirical fitting.

Dynamic Water Erosion Prediction Project

Bulygina *et al.* (2007) developed a dynamic version of the WEPP model, which quantifies the dynamics of sediments within a storm event. This model is based on **Eqs (1)–(6)**. Many equations of sediment transport were developed for stream flow, and later on applied to shallow overland flow and channel flow. According to Alonso *et al.* (1981) and Foster & Meyer, (1972), the Yalin equation applies better for shallow flows associated with upland erosion. In DWEPP, the Yalin flow transport capacity equation is given by:

$$T_c = 0.635 G_s g d \sqrt{\rho_w \tau} \delta \left[1 - \frac{1}{\beta} \ln(1+\beta) \right] \quad (8)$$

$$\delta = \begin{cases} \dfrac{Y}{Y_{cr}} - 1, & Y < Y_{cr} \\ 0, & Y \geq Y_{cr} \end{cases} \quad (9)$$

$$\beta = 2.45 G_s^{-0.4} Y_{cr}^{0.5} \delta \quad (10)$$

$$Y = \frac{\tau}{\rho_w (G_s - 1) g d} \quad (11)$$

where G_s is the particle specific gravity, d the particle diameter (m), δ and β are calculated by **Eqs (8)** and **(9)**, respectively, Y is the dimensionless shear stress from the Shields diagram and Y_{cr} the dimensionless critical shear stress from the Shields diagram.

European Soil Erosion Model

The European Soil Erosion Model (EUROSEM) was developed by Morgan *et al.* (1998). It is based on the **Eqs (1)** and **(2)**, which simulate sediment transport, erosion and deposition over the land surface by rill and interill processes in single storms for both, individual fields and small catchments. Model output for one single storm includes total runoff, total soil loss, hydrographs and sediment graphs. The soil detachment by runoff is modeled in terms of a generalized erosion-deposition theory proposed by Smith *et al.* (1995). According to it, D_R is the flow erosion rate (kg/s/m^2), (positive for erosion and negative for deposition); the flow transport capacity concentration (T_c) represents the sediment concentration at which the flow erosion rate and corresponding deposition rate are in balance. A general equation for flow erosion rate is expressed in terms of the settling velocity and flow transport capacity concentration, as follows:

$$D_R = V_s (T_c - C) \quad (12)$$

The runoff capacity to transport detached soil particles is expressed in terms of the concentration, T_c (kg/m^3) is modeled as a function of unit stream power using the relationship of Govers (1985):

$$T_c = a(\omega - \omega_c)^b \quad (13)$$

$$\omega = VS \quad (14)$$

where ω_c is the critical value of unit stream power, ω the unit stream power (m/s), V_s the particle fall velocity (m/s), a and b are experimentally derived coefficients depending on particle size, S the slope (%) and V the mean flow velocity (m/s).

Erosion model of CIHAM-UC

At the present, an erosion model is being developed at the Centre of Environmental and Hydrologic Research, based on **Eqs (1)–(3)** and **Eq. (15)** of Simons *et al.* (1981), which is based on power relationships that estimate sediment transport based on the flow depth h and velocity V.

These power relationships were developed from a computer solution of the bedload transport equation of Meyer-Peter & Müller, (1948). Guevara & Márquez, (2009) propose it to estimate the sediment transport capacity in rill, and can be expressed as follows:

$$T_c = a h^b V^c \quad (15)$$

where T_c is the flow transport capacity (kg/s/m), a, b and c are parameters estimated by empirical adjustment, V the flow velocity (m/s) and h the flow depth (m).

The flow erosion rate D_R (kg/s/m^2) is described in terms of the generalized theory of erosion-deposition modifying proposal by Smith *et al.* (1995). This condition can be expressed as:

$$DR = T_c / w - f_s C V_s \quad (16)$$

where V_s is the particle fall velocity (m/s), w the furrow width (m), f_s=A_{ec}/$A_{rill,}$ similarity factor, A_{ec} experimental cylinder area from hydrometer test method (D422) (American Society for Testing and Materials, 2007).

Linear Multiple Regression Model

The Linear Multiple Regression Model **(**LMRM) used is based on the structure given by:

$$D_R = \beta_1 P_t + \beta_2 P_{t-1} + \beta_3 P_{t-2} + \ldots + \beta_{12} P_{t-6} \quad (17)$$

where D_R is the flow erosion rate (mg/s/m^2) at time t, β_s represents the regression coefficients to be determined;

intervals within a single storm; and *t* index representing time.

Nonlinear Multiple Regression Model

The Non-Linear Multiple Regression Model **(N**LMRM) used is based on the structure given by:

$$D_R = \beta_1 P^n{}_t + \beta_2 P^n{}_{t-1} + \beta_3 P^n{}_{t-2} + ... + \beta_{12} P^n{}_{t-6} \quad (18)$$

where *n* is the order of polynomial regression. The rest of the variables are explained earlier.

Artificial Neural Networks

Neural networks are composed of simple elements operating in parallel, inspired by biological nervous systems. As in nature, the connections between elements largely determine the network function. A neural network can be trained to perform a particular function by adjusting the values of the connections (weights) between elements. Typically, neural networks are adjusted, or trained, so that a particular input leads to a specific target output. **Figure 1** illustrates such a situation. The network is adjusted, based on a comparison of the output and the target, until the network output matches the target (Demuth *et al.*, 2009).

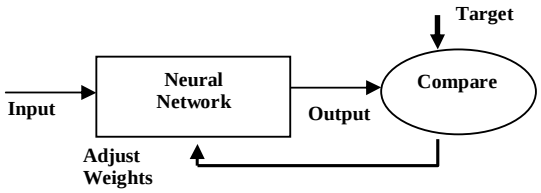

Fig. 1 Scheme Input/Output to ANN.

Neuron Model

One or more of the neurons can be combined in a layer, and a particular network could contain one or more such layers. A one-layer network with *R* input elements and *S* neurons is shown in **Fig. 2** as follows:

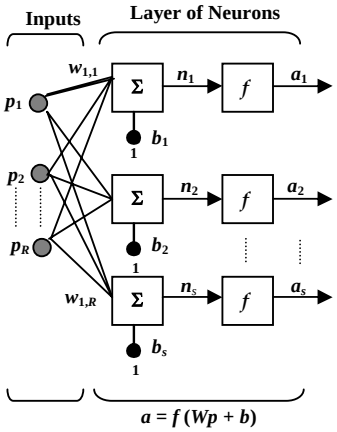

In this network, each element of the input vector ***p*** is connected to each neuron input through the weight matrix ***w***. By considering a neuron with a single *R*-element input vector, *p*, the individual element inputs p_1, p_2,…p_R, are multiplied by weights $w_{1,1}$, $w_{1,2}$, ... $w_{1,R}$ and the weighted values are fed to the summing junction, as shown in **Fig. 2**. This sum is ***Wp***, the dot product of the (single row) matrix ***W*** and the vector ***p***. The neuron has a bias *b*, which is summed with the weighted inputs to form the net input *n*. This sum, *n*, is the argument of the transfer function *f* defined as follows:

$$n = w_{1,1} p_1 + w_{1,2} p_2 + ... + w_{1,R} p_R + b \quad (19)$$

This expression can be written as:

$$n(i) = Wp + b \quad (20)$$

where, the *i*th neuron has a summing that gathers its weighted inputs and bias to form its own scalar output *n* (*i*). The various *n*(*i*) taken together form an *S*-element net input vector ***n***.

The sigmoid transfer function is commonly used in backpropagation networks, in part because it is differentiable. As shown in **Fig. 3**, the sigmoid transfer function takes the input, which can have any value between plus and minus infinity, and squashes the output into the range 0 to 1.

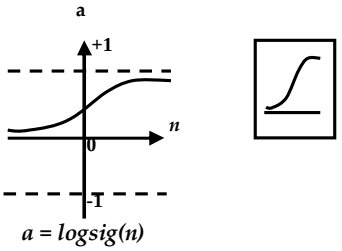

Fig. 3 Log-Sigmoid transfer function.

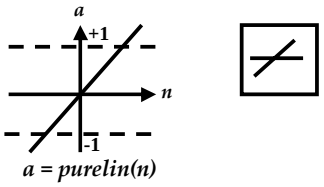

Fig. 4 Lineal transfer function.

Occasionally, the Linear Transfer Function Purelin is used in backpropagation networks. The linear transfer function is illustrated in **Fig. 4**.

The symbol in the square to the right of each transfer function graph shown represents the associated transfer function. These icons replace the general *f* in boxes of network diagrams to show the particular transfer

Feedforward Network

Feedforward networks often have one or more hidden layers of sigmoid neurons followed by an output layer of linear neurons. Multiple layers of neurons with nonlinear transfer functions allow the network to learn nonlinear and linear relationships between input and output vectors. The linear output layer lets the network produce values outside the range –1 to +1. To describe networks having multiple layers, the notation must be extended. Specifically, it needs to make a distinction between weight matrices that are connected to inputs and weight matrices that are connected between layers. A network can have several layers and it uses layer weight (**LW**) matrices as well as input weight (**IW**) matrices. The network shown in **Fig. 5** has R inputs, S^1 neurons in the first layer, and S^2 neurons in the second layer. A constant input 1 is fed to the bias for each neuron. Note that the outputs of each intermediate layer are the inputs to the following layer. Thus layer 2 can be analyzed as a one-layer network with S^1 inputs, S^2 neurons, and an $S^2 \times S^1$ weight matrix W^2. The input to layer 2 is $\boldsymbol{a}^1$; the output is $\boldsymbol{a}^2$. Now that all the vectors and matrices of layer 2 have been identified, it can be treated as a single-layer network on its own. This approach can be taken with any layer of the network.

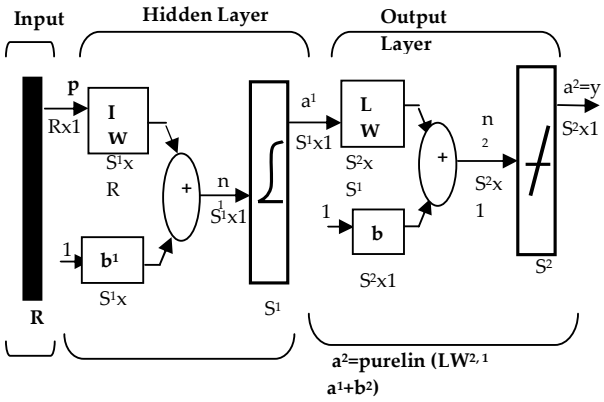

Fig. 5 Archictecture of a feedforward network.

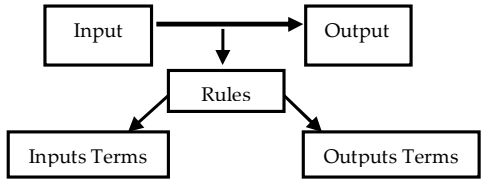

Fig. 6 Diagram of a fuzzy inference system.

Fuzzy Logic

Fuzzy logic has two different meanings. In a narrow sense, fuzzy logic is a logical system, which is an extension of multivalued logic. However, in a wider sense fuzzy logic (FL) is almost synonymous with the theory of fuzzy sets, a theory which relates to classes of objects with unsharp boundaries, in which membership is a matter of degree. The point of fuzzy logic is to map an input space to an output space, and the primary mechanism for doing this is a list of if-then statements called rules. All rules are evaluated in parallel, and the order of the rules is unimportant. The general description of a fuzzy system is shown in **Fig. 6** (MATLAB, 2010).

Fuzzy Inference System

Fuzzy inference is the process of formulating the mapping from a given input to an output using fuzzy logic. The process of fuzzy inference involves three components: (1) membership functions, (2) logical operations and (3) If-Then rules. (1) A ***membership function*** (MF) is a curve that defines how each point in the input space is mapped to a membership value (or degree of membership) between 0 and 1. Membership functions commonly used are as follows: the piece-wise linear functions, the Gaussian distribution function, the sigmoid curve, quadratic and cubic polynomial curves, (2) the ***logical operations***, one particular correspondence between two-valued and multivalued logical operations can be defined by the fuzzy intersection or conjunction (AND), fuzzy union or disjunction (OR), and fuzzy complement (NOT). (3) ***If-Then rules*** are used to formulate the conditional statements that comprise fuzzy logic.

Table 1. Description of study area

Sub-basin	Zone	Geographic Location				Area	Land Use			
		North Coordinate		West Coordinate		(ha)	Agriculture %	Avian %	Domestic %	Other
High	I	10º 13′ 55″	10º 15′ 00″	68º 12′ 10″	68º 11′ 05″	244.38	95.30	2.70	2	0
	II	10º 13′ 00″	10º 14′ 00″	68º 11′ 10″	68º 12′ 00″	209.21	87.99	4.46	6.13	1.42
Medium	III	10º 10′ 10″	10º 11′ 50″	68º 11′ 10″	68º 10′ 20″	320.64	93.04	0.74	6.22	0
	IV	10º 11′ 50″	10º 12′ 20″	68º 11′ 30″	68º 10′ 30″	162.58	77.78	5.56	16.66	0
Low	V	10º 12′ 25″	10º 13′ 10″	68º 11′ 10″	68º 11′ 50″	131.74	83.33	5.56	16.67	0
	VI	10º 12′ 18″	10º 15′ 45″	68º 11′ 67″	68º 15′ 07″	250.64	94.04	0.84	7	0
Percentage Average							88.58	3.31	9.11	0.24
Total						1319.19	1169	44	120	3.16

Two types of fuzzy inference systems can be implemented: Mamdani-type and Sugeno-type. These two types of inference systems vary somewhat in the way outputs are determined. In this investigation Sugeno-type system is used, which can be used to model any inference system in which the output membership functions are either linear or constant.

Fuzzy Modeling Scenario

To apply fuzzy inference to a system for which a collection of input/output data models, a model structure based on characteristics of variables in a system does not necessarily have been predetermined. In some modeling situations, the membership functions cannot be discerned from looking at data. Rather than choosing the parameters associated with a given membership function arbitrarily, these parameters could be chosen so as to tailor the membership functions to the input/output data in order to account for these types of variations in the data values. In such cases, *neuro-adaptive* learning techniques incorporated in the ANFIS command of MATLAB can be used. The acronym ANFIS derives its name from *adaptive neuro-fuzzy inference system*. Using a given input/output data set, the toolbox function ANFIS constructs a fuzzy inference system (FIS) whose membership function parameters are tuned (adjusted) using either a backpropagation algorithm alone or in combination with a least squares type of method. This adjustment allows to fuzzy systems to learn from the data they are modeling.

FIS structure and parameter adjustment A network-type structure similar to that of a neural network, which maps inputs through input membership functions and associated parameters, and then through output membership functions and associated parameters to outputs, can be used to interpret the input/output map. The parameters associated with the membership functions changes through the learning process. The computation of these parameters (or their adjustment) is facilitated by a gradient vector. This gradient vector provides a measure of how well the fuzzy inference system is modeling the input/output data for a given set of parameters. When the gradient vector is obtained, any of several optimization routines can be applied in order to adjust the parameters to reduce some error measure. This error measure is usually defined by the sum of the squared difference between actual and desired outputs. ANFIS uses either back propagation or a combination of least squares estimation and backpropagation for membership function parameter estimation.

MATERIALS AND METHODS

Measurements were made in Chirgua River Basin, located in the north central region of Venezuela during 2008–2009. Each subbasin was divided into zones, which were classified as follows: high: I and II, medium: III, low: IV, V and VI. Each zone is mainly used for agricultural purposes. Information on the location, area and land use is shown in **Table 1**. Five fields were selected with the following slopes in tillage orientation: 0.008 ± 0.0055 m/m; 0.01 ± 0.00197 m/m; 0.015 ± 0.0006 m/m; 0.025 ± 0.0033 m/m and 0.13 ± 0.0156 m/m, whose soils range from silty sand to silty clay. Two types of crops usually are grown in rotation, according to the season: dry (potato: Solanum Tuberosum) and rainy (corn: *Zea Mays*); whose development cycles have the following time periods: 12 and 18 weeks, respectively.

The irrigation events for the whole cycle lasted as follows: two hours for the first ten weeks and one hour for the last two weeks. A sprinkler irrigation system was used to provide water to crops. The inflow rate that was applied to furrows varied between 0.4 and 0.6 L/s. A plot of 64 wheel-compacted furrows on each field was split into eigth, 8-furrow blocks. The tests were carried out in three furrows with a width and length as varied as follows: 0.3 and 0.35 m; 100 and 200 m, respectively. Furrows were divided into four equal-length sections (¼, ½, ¾, and at the end of the furrow), and measurement stations were established at the downstream end of each section. Flows were measured using a steel plate with a 60º V-notch weir, by applying the volumetric method. The number of measurements carried out during the dry and rainy seasons were 300 and 162, respectively, which included: a) Soil physical properties: undisturbed samples were captured to determine through laboratory analysis saturated hydraulic conductivity, specific gravity, shear stress, moisture content, Atterberg limits and particle size (hydrometer and sieve analysis). Infiltration rates were measured with a single-ring infiltrometer (diameter 30 cm), which was driven up to 5 cm deep into the soil. (**Table 2** and **Fig. 7**), b) Flow physical properties: flow rates and sediment concentrations were measured at time intervals ranging from 20 to 120 min at a time, after the arrival of water to each measuring station. Sediment concentration was determined by applying the 2 540 B method (American Public Health Association, 1995). 120 irrigation events were measured in five different agricultural fields (5 fields × 24 events / field = 120 irrigation events). During the rainy season the following events were measured: 73 for 2 hours, 24 for an hour and 20 for half an hour, with a precipitation gauge attached to an electronic storage unit, which has following geographic location: °W 68º 10’ 50’’and °N 10º 11’ 45’’. Total data were divided into three

groups: 60% for calibration, 20% for validation and 20% for testing.

Models data

Table 2 shows soil physical properties. Soil is composed of soil particles, where approximately less than 3% represents < 2.00 mm, 46.1% represents < 0.074 mm (fine fraction) and 50.9% represents >0.074 mm (finest fraction: silt and clay). Saturated hydraulic conductivity is close to 1 mm/h in most areas, which is classified as low to lower (Terzaghi & Peck, 1967). The friction angle varies from 29.8 to 32.7º. The cohesion varies from 0.1 to 0.43 kgf/cm^2. The initial and final moisture contents of the soil vary from 7.1 to 21.8%; from 26.1 to 54%, respectively. The porosity varies from 0.4 to 0.5 cm^3/cm^3. The liquid limit, plastic limit and plasticity index range respectively as follows: 26.2 and 33.2%; 23 and 28%; 4.3 and 5.2%. Specific gravity of solids varies from 2.5 to 2.6. Soil type varies from organic silt (OL) to plasticity low silty sand (SM) (e.g., Lambe & Whitman, 1972; Juarez & Rico, 1991) (**Table 2**).

Infiltration rates for silty soil are highly variable. **Figure 7(a)** shows the cumulative infiltration versus time for 582 infiltrometer tests over one period, which last 2.28 h each. Infiltration depths at the end of this time have a mean of 22.39 mm and a standard deviation of 21.02 mm. Infiltration depths greater than 22.39 mm are measured during the rainy season, where rainfall events occur less frequently than those of irrigation, therefore the storage capacity of the soil is higher than those available during the irrigation period. **Figure 7(b)** shows the histogram for the cumulative infiltration at t = 2.28 h, together with the corresponding probability density functions. Exponential and Weibull functions result in the best fit.

Table 2. Soil physical properties

Soil physical Properties	Zone																	
	I			II			III			IV			V			VI		
	μ	σ	CV	μ	σ	CV	μ	σ	CV	μ	σ	CV	μ	σ	CV	μ	σ	CV
Texture																		
PRetained Percentage on Sieve																		
>9.51mm (Sieve 3/8″)	3.9	4.4	112.9	0.0	0.0	-	1.2	1.1	93.2	1.2	1.5	126.5	0.0	0.0	-	0.3	0.5	146.9
9.51 – 4.76 mm (Sieve # 4)	2.6	1.9	70.1	4.0	4.5	110.6	1.3	0.8	63.3	1.4	1.3	94.1	0.9	0.3	38.2	2.2	2.1	96.8
4.76 – 2.00 mm (Sieve # 10)	4.0	2.5	61.8	5.5	5.3	95.3	2.7	1.1	39.0	2.7	1.5	55.9	3.7	2.8	75.9	0,7	1.3	188.2
2.00 – 0.84 mm (Sieve # 20)	6.7	3.6	54.0	10.9	7.8	71.7	5.7	2.1	36.5	5.6	2.0	34.9	8.3	4.1	49.2	7.2	3.5	48.2
0.84 – 0.42 mm (Sieve # 40)	10.9	5.2	47.3	14.5	6.4	44.2	8.7	2.8	32.1	8,3	1.8	22.1	13.8	3.9	28.7	10.4	3.7	36.1
0.42 – 0,149 mm (Sieve # 100)	22.6	5.2	23.0	31.2	9.8	31.6	15.7	2.9	18.4	18.8	3.1	16.4	19.0	3.3	17.5	32.5	8.0	24.7
0.149 – 0.074 mm (Sieve #200)	14.4	6.3	43.8	28.3	12,6	44.6	13.0	3.4	26.1	15.1	2.5	16.6	15.7	5.1	32.2	28.5	11.5	40.2
< 0.074 mm Plate	34.9	9.3	26.6	5.9	3.5	60.3	51.7	9.5	18.4	48.2	8.6	17.9	38.7	7.8	20.2	18.3	12.0	65.8
Total Percentage Average																		
Sand (%)	46.4	4.2	9.1	30.7	5.6	18.4	46.1	1.6	3.5	46.2	2.1	4.6	46.1	1.6	3.5	46.1	1.6	3.5
Silt (%)	49.5	2.7	5.5	36.7	11.7	31.9	46.9	2.3	4.9	46.9	2.3	4.9	49.5	2.7	5.5	46.9	2.3	4.9
Clay (%)	4.1	2.0	48.4	19.9	8.2	41.3	7.0	2.4	33.9	6.9	2.5	36.2	6.6	1.8	27.6	7.0	2.4	33.9
Hydraulic Properties																		
K_s[1] (mm/h)	0.4	0.1	33.3	24.0	22.7	94.3	0.9	0.6	60.6	1.4	0.6	41.8	0.9	0.6	60.6	0.9	0.6	60.6
Structural Properties																		
Friction Angle (º)	29.9	3.9	12.9	29.8	1.1	3.8	29.8	1.1	3.8	32.7	1.1	3.4	31.8	1.9	5.9	32.7	1.1	3.4
Cohesion (kgf/cm^2)	0.3	0.0	15.4	0.1	0.0	60.0	0.1	0.0	60.0	0.3	0.0	6.7	0.43	0.03	7.0	0.3	0,0	6.7
Phase Relations																		
Initial moisture content (%)	21.8	11.5	52.6	7.1	3.5	49.2	18.9	11.8	62.5	15.0	7.1	47.2	20.7	10.6	51.3	18.9	11.8	62.5
Final moisture content (%)	26.1	11.5	44.0	51.0	11.7	22.9	40.5	7.7	19.0	54.0	12.6	23.4	40.5	7.7	19.0	40.5	7.7	19.0
Porosity (cm^3/cm^3)	0.4	0.1	13.5	0.4	0.1	11.6	0.4	0.1	14.6	0.4	0.1	18.9	0.5	0.1	16.7	0.4	0.1	14.6
Liquid limit (%)	26.2	2.5	9.4	30.7	4.1	13.3	32.4	4.4	13.4	29.6	2.0	6.8	33.2	4.2	12.8	32.4	4.4	13.4
Plastic limit (%)	23.1	5.0	21.6	26.2	3.7	14.0	27.1	2.9	10.6	25.2	3.4	13.6	28.3	3.9	13.9	27.1	2.9	10.6
Plasticity index (%)	5.1	2.2	43.8	4.5	2.5	54.3	5.2	4.0	76.0	4.3	2.6	60.0	4.9	1.2	25.0	5.2	4.0	76.0
Specific gravity	2.6	0.1	3.9	2.5	0.1	4.8	2.5	0.1	4.3	2.6	0.2	7.7	2.7	0.1	3.7	2.5	0.1	4.3

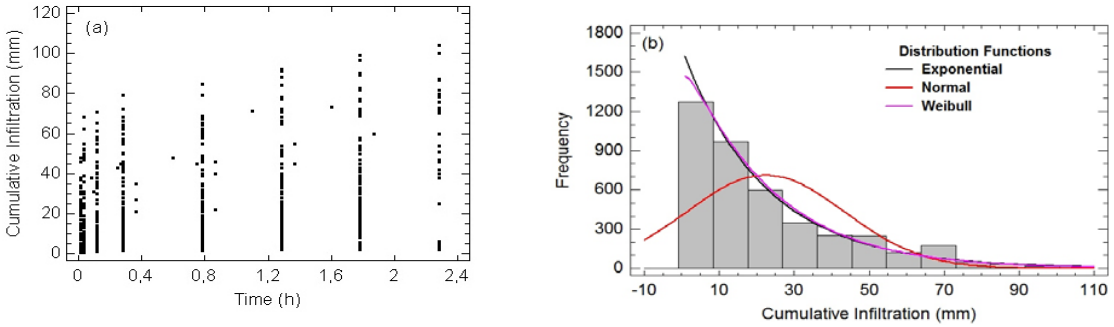

Fig. 7 Cumulative infiltration depth: (a) temporal variation, and (b) frequency histogram and predicted Weibull probability density function.

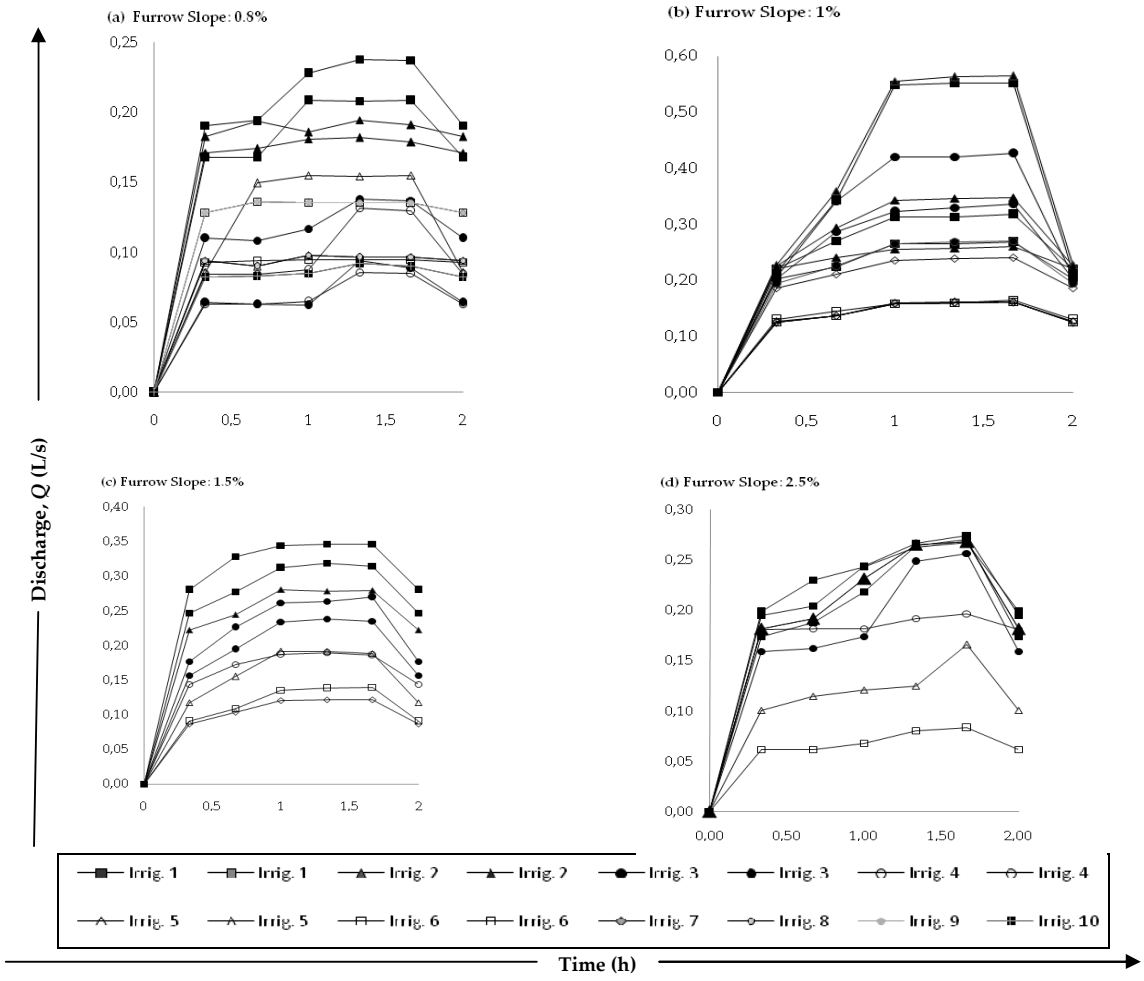

Fig. 8 Measured hydrographs for different slope furrows during each irrigation.

During the dry season, runoff is stabilized after the first half hour when the irrigation is applied. The time for flow stabilization is approximately one hour; which occurs faster in the furrows where the slope was equal to 0.8% (**Fig. 8**). Flow rate at steady state varies from 0.3 to 0.5 L/s, decreasing from 0.05 to 0.1 L/s after the seventh irrigation. The effect of the coverage radio of the sprinkler on flow varying between the different furrows is low within an irrigation event.

A comparison of the sediment load during irrigation and rain events of one and two hours is shown in **Fig. 9**. The maximum sediment load observed during the irrigation and rainfall events of one hour varies approximately from 100 to 400 mg/s, from 600 to

sediment load observed for the two-hour event varies from 500 to 2000 mg/s for irrigation and from 2500 to 7000 mg/s for rain (**Fig. 9(b)**). Therefore, there is significant variation in sediment load between the events of rain and irrigation, where the first is 5 to 10 times more erosive than the latter.

A comparison of rainfall events in both one and two hours is shown in **Fig. 10**, which shows that the rainfall for these events ranges as follows: from 20 to 30 mm, and from 25 to 40 mm, respectively (**Figs 10(a)** and **(b)**).

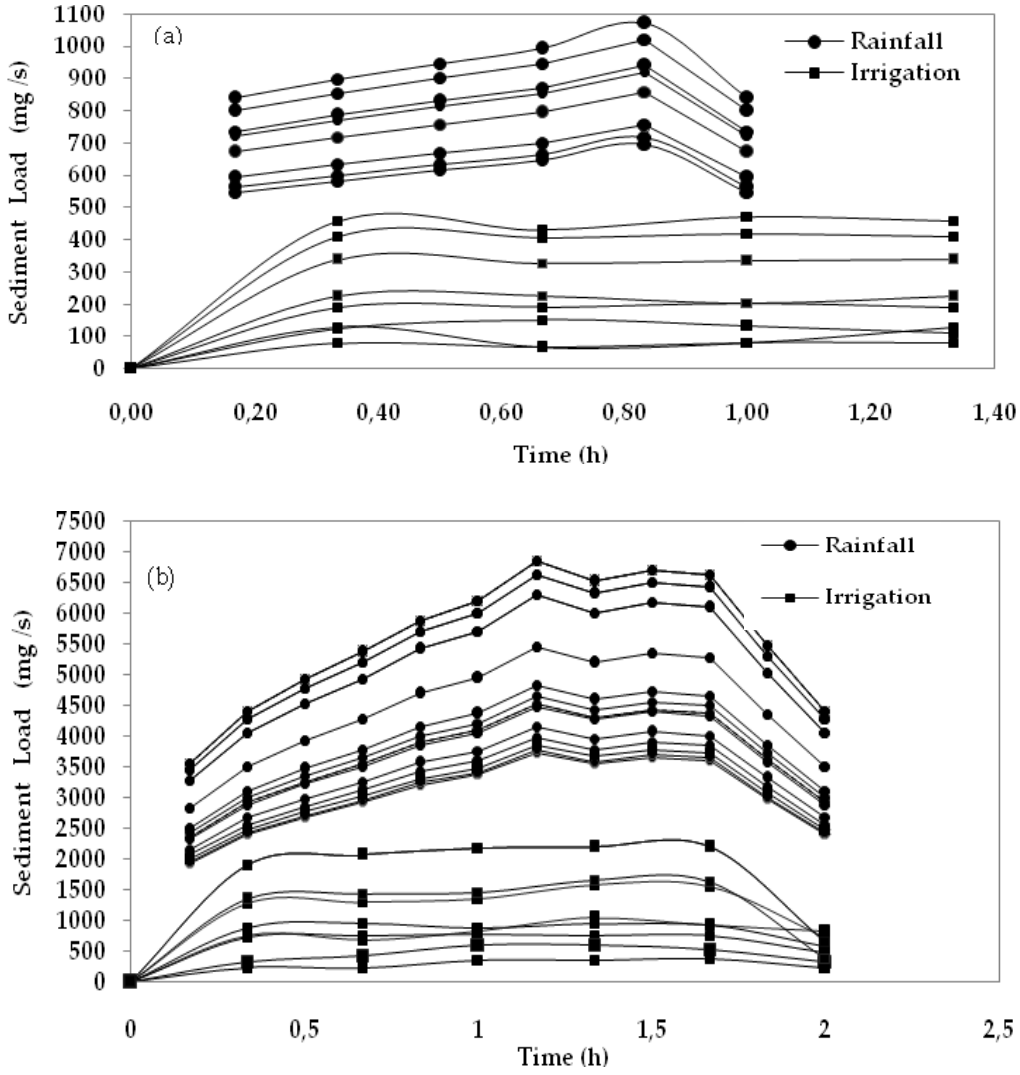

Fig. 9 Measured sediment load during rainfall and irrigation events.

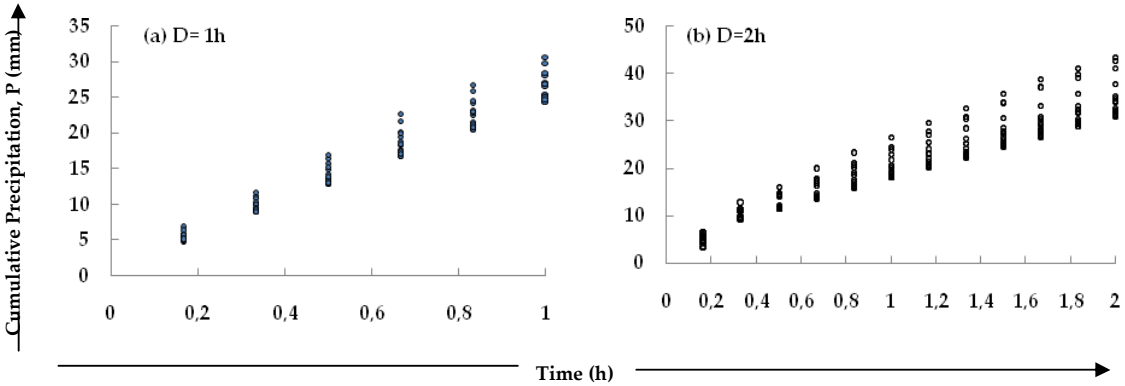

Fig. 10 Precipitation depth

RESULTS

Modeling of furrow erosion based on physical processes

Process of particle detachment

Table 3 shows the parameters of **Eq. (5)**, used to estimate the capacity of soil particle detachment in furrows. In general, the following statements can be made about the parameters K_c and τ_c: (a) K_c varies from 1.31E–06 to 1.525E–06 s m^{-1}; (b) τ_c varies from 0.704 to 1.489 Pa; (c) estimate standard error of the parameters is low in all cases.

Table 4 shows fit statistics of **Eq. (5)** to the observations obtained from field testing in the furrows of different slopes. The results are summarized as follows: R^2 is equal to 0.682, $R^2_{adj.}$ is equal to 0.681, its reduction is not significant in relation to R^2. Mallows C_p decreases slightly compared to the number of independent variables in **Eq. (5)**. Durbin-Watson statistic is equal to 0.66. By comparing the errors during the calibration and validation stages, with emphasis on the Average Absolute Relative Error (AARE), and the Average Relative Error (ARE) the following results are found: AARE varies from 47.87 to 57.9, ARE varies from –20.52 to –33.74. In general, the errors do not vary significantly between the stages of calibration and validation. The rest of errors can be seen in **Table 4**.

Process of sediment transport

Table 5 shows the parameters of **Eqs 7**, **13** and **15** for estimating the sediment transport capacity in furrows. In general, the following statements can be made about the parameters K_t, b and c: **Coefficient of transport (K_t):** (a) the units differ between **Eqs 7**, **13** and **15**, (b) the ranges found for **Eqs 7**, **13** and **15** vary as follows: 9.929E–08 and 1.526E–07; 7.634 and 34.583; 0.421 and 0.892, respectively, (c) estimate standard error of parameters is moderately low in all cases. **Parameter *b*:** (a) the ranges found for **Eqs 7**, **13** and **15** vary as follows: 1.519 and 1.705; 0.398 and 1.299; 2.087 and 2.228; respectively, (b) estimate standard error of parameters is low in all cases. **Parameter *c*:** (a) the range found for **Eq. (15)** varies from 1.097 to 1.193; (b) estimate standard error of parameters is low in all cases.

Table 6 shows fit statistics of **Eqs 7**, **13** and **15** to the observations obtained from field testing in the furrows. R^2: varies from 0.72 to 0.88. $R^2_{adj.}$: its reduction is not significant in relation to R^2. Mallows C_p: decreases slightly compared to the number of independent variables in each equation. Durbin-Watson statistic: values found to **Eqs 7**, **13** and **15** are equal to 0.719, 1.09 and 0.74, respectively. By comparing the errors during the calibration and validation stages with emphasis on the Average Absolute Relative Error (AARE) and the Average Relative Error (ARE) the following results in **Eqs 7**, **13** and **15** are found: AARE varies from 56.319 to 63.081; from 12.125 to 13.482; from 29.585 to 29.894. ARE varies from –13.365 to –1.831; from –1.831 to 1.974; from –16.597 to –18.547. In general, the errors do not vary significantly between calibration and validation stages. The rest of errors can be seen in **Table 6**.

Combination of furrow erosion processes

The representation of furrow erosion processes for following slopes: 0.8%, 1%, 1.5% and 2.5% is shown in **Fig. 11**, using the **Eqs 7**, **13** and **15** for estimating the transport capacity of sediments **(Figs 11a**, **11c**, **11e** and **11h**, and **Eqs 4** and **12** to estimate the net detachment capacity (**Figs 11b, 11d, 11f** and **11g**). The cycle under irrigation has been divided into three stages; each stage represents 1/3 of the total duration for 12 weeks, obtaining data average values for each phase.

Table 3. Regression coefficients of particle detachment capacity model

Eq.	Variable	Parameter	Unit	Average	Standard Error	Minimum Limit	Maximum Limit
5	D_c	K_r	s/m	0.000 001 418	5.43 497E–8	0.00 000 131 163	0.000 0015 255
	(kg/s/m^2)	τ_c	Pa	1.09 707	0.199 697	0.704 172	1.48 997

Table 4. Performance criteria of particle detachment capacity model

Eq.	p	n	R^2	$(R^2)_{adj.}$	C_p	SEE	d	MSSE	AAE	AARE	AE	ARE	n	AARE	ARE
(a) During Calibration													(b) During Validation		
5	1	320	0.682	0.681	0	2.45E–6	0.66	6.04E–12	2.08E–06	47.87	–7.72E–13	–20.52	84	57.9	–33.74

Eq.: equation; p: number of independent variables in the model; n: number of observed data; R^2: determination coefficient; $(R^2)_{adj.}$: adjusted determination coefficient; C_p: coefficient of Mallows; SEE: Standard error of estimate; d: statistic of Durbin-Watson; MSSE: mean of sum of squared error; AAE: average absolute error; AARE: average absolute relative error (%); AE: average error; ARE: average relative error (%).

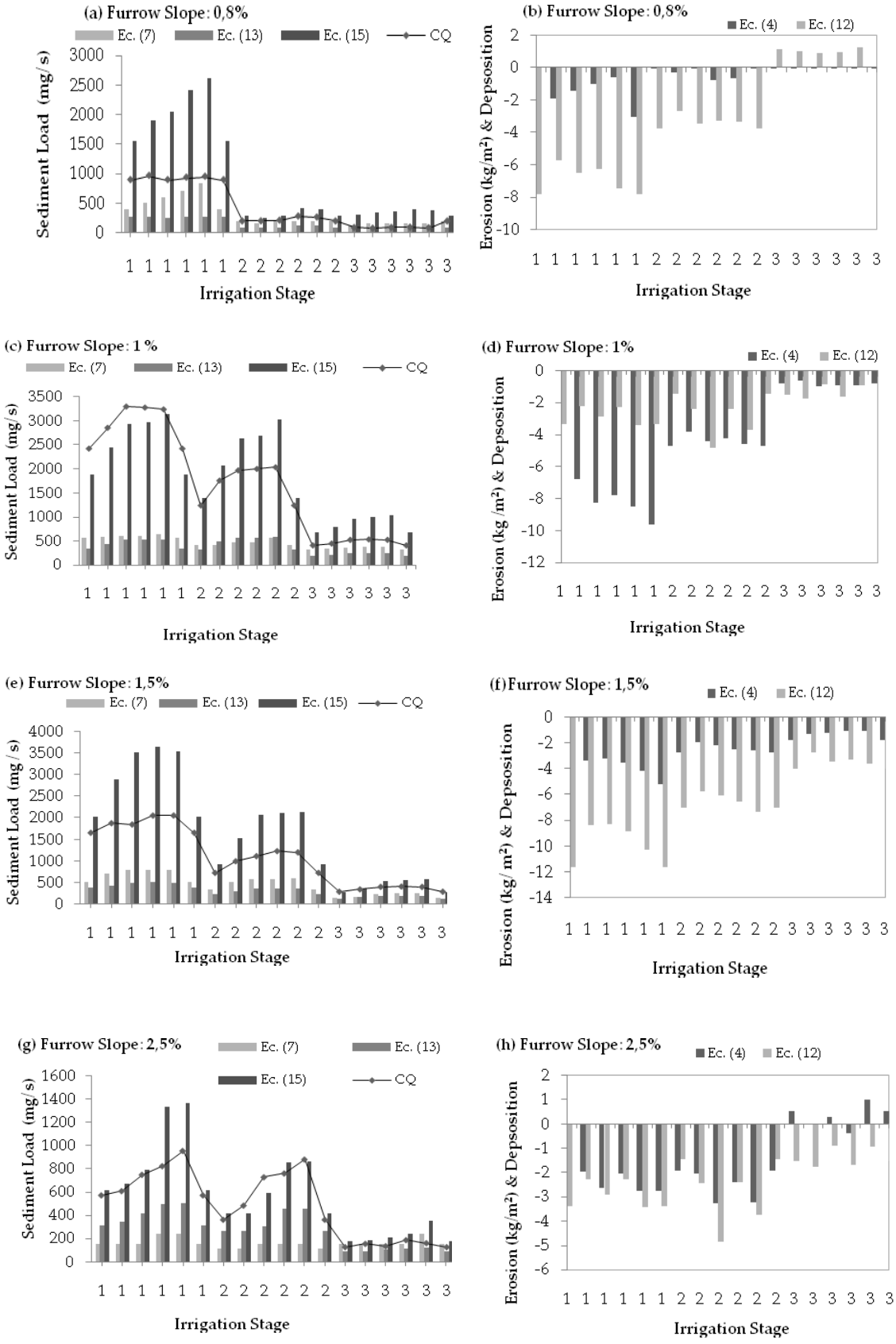

Fig. 11 Comparisons of simulated furrow erosion processes with observed data.

Table 5. Regression coefficients of sediment transport capacity model

Eq.	Variable	Parameter	Unit	Average	Standard Error	Minimum Limit	Maximum Limit
7	T_c	K_t	$kg^{1-b}\ m^{-(1-b)}\ s^{-(1-2b)}$	1.2598E–7	1.35 793E–8	9.92 906E–8	1.52 669E–7
	kg/m/ s	b		1.61 238	0.0 473 371	1.51 934	1.70 542
13	T_c	K_t	$kg\ m^{-(b+1)}\ s^{-(1-b)}$	21.1093	6.843	7.634	34.583
		b		0.8489	0.2287	0.3985	1.2993
	kg/m/s	ω_c	$m\ s^{-1}$	–0.05 414	0.0221	–0.0978	–0.0104
15	T_c	K_t	$kg\ m^{(-1-b-c)}\ s^{-(1+b)}$	0.657 032	0.120 287	0.421 274	0.89 279
		b		2.15 807	0.0 359 035	2.0877	2.22 844
	kg/m/ s	c		1.14 551	0.0 244 874	1.09 751	1.1935

Table 6. Performance criteria of sediment transport capacity model

Eq.	p	n	R^2	R^2_{adj}	C_p	SEE	d	MSSE	AAE	AARE	AE	ARE	n	AARE	ARE
(a) During Calibration													(b) During Validation		
7	1	437	0.73	0.732	0	1.102E–06	0.719	1.22E–12	9.16E–07	63.08	4.24E–08	–31.831	100	56.31	–13.36
13	1	320	0.72	0.720	0	0.34	1.09	0.115	0.287	12.12	0.0028	–1.831	96	13.48	1.974
15	2	700	0.88	0.882	1	1.644E–06	0.741	2.70E–12	1.08E–06	29.58	–5.75E–08	–16.597	165	29.89	–18.54

Comparison between the transport capacities of sediments observed and estimated by **Eqs 7**, **13** and **15** shows in **Figs 11a, 11c, 11e** and **11h**. The solid line represents the observed sediment load in furrows, while the bars represent estimates by **Eqs 7**, **13** and **15**, where the following observations can be made: (a) **Eq. (13)** overestimated the values of the observed transport capacity, but the rest of equations underestimated them and (b) the observed sediment load in stages from 1 to 3 varies as follows: from 1000 to 2500 mg/s, from 2000 to 500 mg/s; less than 500 mg/s.

Values estimated by **Eq. (7)** in stages from 1 to 3 vary as follows: from 500 to 1000 mg/s, from 0 to 500 mg/s, less than 500 mg/s. Values estimated by **Eq. (13)** in stages from 1 to 3 vary as follows: from 1000 to 2500 mg/s, from 2000 to 500 mg/s, less than 500 mg/s. Estimates from **Eq. (15)** in steps 1 through 3 vary as follows: from 1500 to 3500 mg/s, from 500 to 2000 mg/s, from 500 to 1000 mg/s, (c) the difference between observed and estimated values is significant in the first stage of the cycle and decreases towards the second and third stages.

According to the theory of models based on physical processes, when the sediment transport capacity is exceeded by the flow sediment load occurs the deposition process (Foster and Meyer, 1975, Morgan *et al.*, 1998).

Deposition process estimated by **Eqs 4** and **12** is shown in **Figs 11(b)**, **11(d)**, **11(f)** and **11(g)**, where the following results determine: (a) most times **Eq. (12)** estimates higher values than **Eq. (4)**, (b) the estimated values by **Eq. (4)** in the stages from 1 to 3 vary as follows: from 2 to 6 kg/m^2, from 0 to 4 kg/m^2, from 0 to 2 kg/m^2, respectively. Estimates from **Eq. (12)** in stages from 1 to 3 vary as follows: from 6 to 12 kg/m^2, from 2 to 6 kg/m^2, from 2 to 4 kg/m^2, (c) the difference between observed and estimated values is significant during the first stage of the cycle and decreases towards the second and third stages.

Modeling furrow erosion based on regressions

Table 7 shows the parameter values in the furrow erosion models based on linear regressions, **Eqs 17(a)** and **(b)**, as well as nonlinear regressions, **Eqs 18(a)–(e)**. In general, the following statements can be made in relation to the parameters β_1 to β_6: in **Eq. (17a)** the parameters vary from –4.267 to 4.382, in **Eq. (17b)** they vary from –7.5 to 9.14, in **Eq. (18a)** they vary from –0.031 and 0.2697, in **Eq. (18b)** they vary from –0.014 to 0.093, in **Eq. (18c)** they vary from –0.629 to 1.938, in **Eq. (18d)** they vary from –0.046 to 1.012.

Table 8 shows the fitted statistics of erosion models based on regression from the observations obtained when the field was examined in furrows, in the following slopes: 0.8%, 1%, 1.5%, and 2.5%. R^2: varies from 0.90 to 0.53, and it decreases when the polynomial power is increased. R^2_{adj} its reduction is not significant in relation to R^2. **Mallows C_p**: decreases slightly compared to the number of independent variables in each equation**. Durbin-Watson Statistics**: varies between 0.7 and 1.68. By comparing the errors during the calibration and validation stages, with emphasis on the average absolute relative error (AARE), and the average relative error (ARE) the following results are found: AARE varies from 6.21 to 12.57, ARE varies from –0.71 to 6.78. In general, (a) errors tended to be lower in the calibration stage with respect to validation and (b) errors increase when the polynomial power is increased. The rest of errors can be seen in **Table 8**.

Figure 12 shows a comparison of the estimated erosion results using **Eqs 17(a)**, **17(b)**, **18(a)**, **18(b)**, **18(c)** and **18(d)** to the observations under irrigation in the furrows with following slopes: 0.8%, 1%, 1.5% and 2.5%. Additionally, it includes a comparison with the physical process model represented by **Eq. (16)**, and the artificial intelligence technique based on neural networks, which will be widely discussed in the next section.

Table 7. Regression coefficients of erosion model based on LMR and NLMR

Eq.	Dependent variable	Independent variable	Parameter	Unit	Average	Standard Error	Minimum Limit	Maximum Limit
17(a) LMRM *n*=1 D=1H	D_r mg m^{-2} s^{-1}	Pt	β_1	mg m^{-2} s^{-1} mm^{-1}	1.398583862	1.442760413	–4.267676785	1.47050906
		Pt-1	β_2	mg m^{-2} s^{-1} mm^{-1}	0.833406797	1.784933149	–2.716135469	4.382949064
		Pt-2	β_3	mg m^{-2} s^{-1} mm^{-1}	0.731227333	1.392642416	–2.03820026	3.500654927
		Pt-3	β_4	mg m^{-2} s^{-1} mm^{-1}	0.183129882	1.814769332	–3.425745022	3.792004785
		Pt-4	β_5	mg m^{-2} s^{-1} mm^{-1}	0.737812187	1.250395401	–1.748741065	3.224365439
		Pt-5	β_6	mg m^{-2} s^{-1} mm^{-1}	0.559520883	0.731816989	–0.895780305	2.014822071
17(b) LMRM *n*=1 D=2H	D_r mg m^{-2} s^{-1}	Pt	β_1	mg m^{-2} s^{-1} mm^{-1}	0.794050629	1.4177439	–3.585879266	1.997778008
		Pt-1	β_2	mg m^{-2} s^{-1} mm^{-1}	2.195990758	2.69409942	–7.5012253	3.109243783
		Pt-2	β_3	mg m^{-2} s^{-1} mm^{-1}	0.780383734	3.769700299	–6.642929634	8.203697103
		Pt-3	β_4	mg m^{-2} s^{-1} mm^{-1}	2.177019018	1.357605748	–0.496385258	4.850423294
		Pt-4	β_5	mg m^{-2} s^{-1} mm^{-1}	4.541647609	2.338266456	–0.062878815	9.146174033
		Pt-5	β_6	mg m^{-2} s^{-1} mm^{-1}	0.099997046	0.333760338	–0.557245543	0.757239634
18(a) NLMR M *n*=2 D=1H	D_r mg m^{-2} s^{-1}	Pt	β_1	mg m^{-2} s^{-1} mm^{-1}	0.119031048	0.073909116	–0.031707895	0.269769991
		Pt-1	β_2	mg m^{-2} s^{-1} mm^{-1}	0.055276888	0.084390798	–0.116839631	0.227393406
		Pt-2	β_3	mg m^{-2} s^{-1} mm^{-1}	0.066816629	0.061319061	–0.058244676	0.191877933
		Pt-3	β_4	mg m^{-2} s^{-1} mm^{-1}	0.050906233	0.084917164	–0.122283818	0.224096283
		Pt-4	β_5	mg m^{-2} s^{-1} mm^{-1}	0.075651656	0.055759098	–0.038070006	0.189373318
		Pt-5	β_6	mg m^{-2} s^{-1} mm^{-1}	0.05458908	0.025644464	0.002286744	0.106891417
18(b) NLMR M *n*=3 D=1H	D_r mg m^{-2} s^{-1}	Pt	β_1	mg m^{-2} s^{-1} mm^{-1}	0.065622334	0.013487094	0.038182579	0.093062088
		Pt-1	β_2	mg m^{-2} s^{-1} mm^{-1}	0.014849305	0.014240642	–0.014123558	0.043822168
		Pt-2	β_3	mg m^{-2} s^{-1} mm^{-1}	0.002274855	0.007430699	–0.012843047	0.017392756
		Pt-3	β_4	mg m^{-2} s^{-1} mm^{-1}	0.01600253	0.014611824	–0.013725509	0.045730568
		Pt-4	β_5	mg m^{-2} s^{-1} mm^{-1}	0.008392722	0.009444179	–0.010821644	0.027607088
		Pt-5	β_6	mg m^{-2} s^{-1} mm^{-1}	0.006471389	0.003122043	0.000119533	0.012823245
18 (c) NLMR M *n*=2 D=2H	D_r mg m^{-2} s^{-1}	Pt	β_1	mg m^{-2} s^{-1} mm^{-1}	0.565467014	0.170384074	0.227999229	0.902934798
		Pt-1	β_2	mg m^{-2} s^{-1} mm^{-1}	0.060856563	0.260216264	–0.454535539	0.576248665
		Pt-2	β_3	mg m^{-2} s^{-1} mm^{-1}	1.110633143	0.418014423	0.282701296	1.938564991
		Pt-3	β_4	mg m^{-2} s^{-1} mm^{-1}	0.334619992	0.145250564	0.046932389	0.622307595
		Pt-4	β_5	mg m^{-2} s^{-1} mm^{-1}	–1.53E–01	0.240668154	–0.629188284	0.324160779
		Pt-5	β_6	mg m^{-2} s^{-1} mm^{-1}	0.042533197	0.020393795	0.002140637	0.082925756
18(d) NLMR M *n*=3 D=2H	D_r mg m^{-2} s^{-1}	Pt	β_1	mg m^{-2} s^{-1} mm^{-1}	0.305101494	0.068845599	0.168692499	0.44151049
		Pt-1	β_2	mg m^{-2} s^{-1} mm^{-1}	0.1154	0.0815	–0.0460	0.2769
		Pt-2	β_3	mg m^{-2} s^{-1} mm^{-1}	0.691301164	0.161871969	0,370571984	1.012030344
		Pt-3	β_4	mg m^{-2} s^{-1} mm^{-1}	0.08363529	0.049106013	–0.013662171	0.18093275
		Pt-4	β_5	mg m^{-2} s^{-1} mm^{-1}	–0.3610	0.0819	–0.5233	–0.1988
		Pt-5	β_6	mg m^{-2} s^{-1} mm^{-1}	0.01057652	0.003464163	0.003712711	0.017440329

Table 8. Performance criteria of erosion model based on LMR and NLMR

Eq.	Order	*D*	*p*	*N*	R^2	$(R^2)_{adj}$	*Cp*	SEE	*d*	MSSE	AAE	AARE	AE	ARE	*n*	AARE	ARE
(a) During Calibration															(b) During Validation		
17(a)	1	1	6	90	0.900	0.894	5	2.85	0.146	8.179	2.121						
17(b)	1	2	6	264	0.895	0.893	5	4.22	0.160	17.874	3.179						
18(a)	2	1	6	37	0.717	0.672	5	0.78	0.181	0.609	0.593	7.184	0.0008	–0.71	8	9.09	6.78
18(b)	3	1	6	39	0.705	0.660	5	0.84	0.708	0.909	0.708	8.486	0.0024	–0.78	6	6.21	–2.31
18(c)	2	2	6	122	0.725	0.713	5	1.50	0.945	2.252	1.183	10.060	0.0685	–0.45	10	6.83	4.06
18(d)	3	2	6	118	0.538	0.518	5	1.90	1.680	3.626	1.430	11.859	0.2065	0.90	14	12.57	3.31

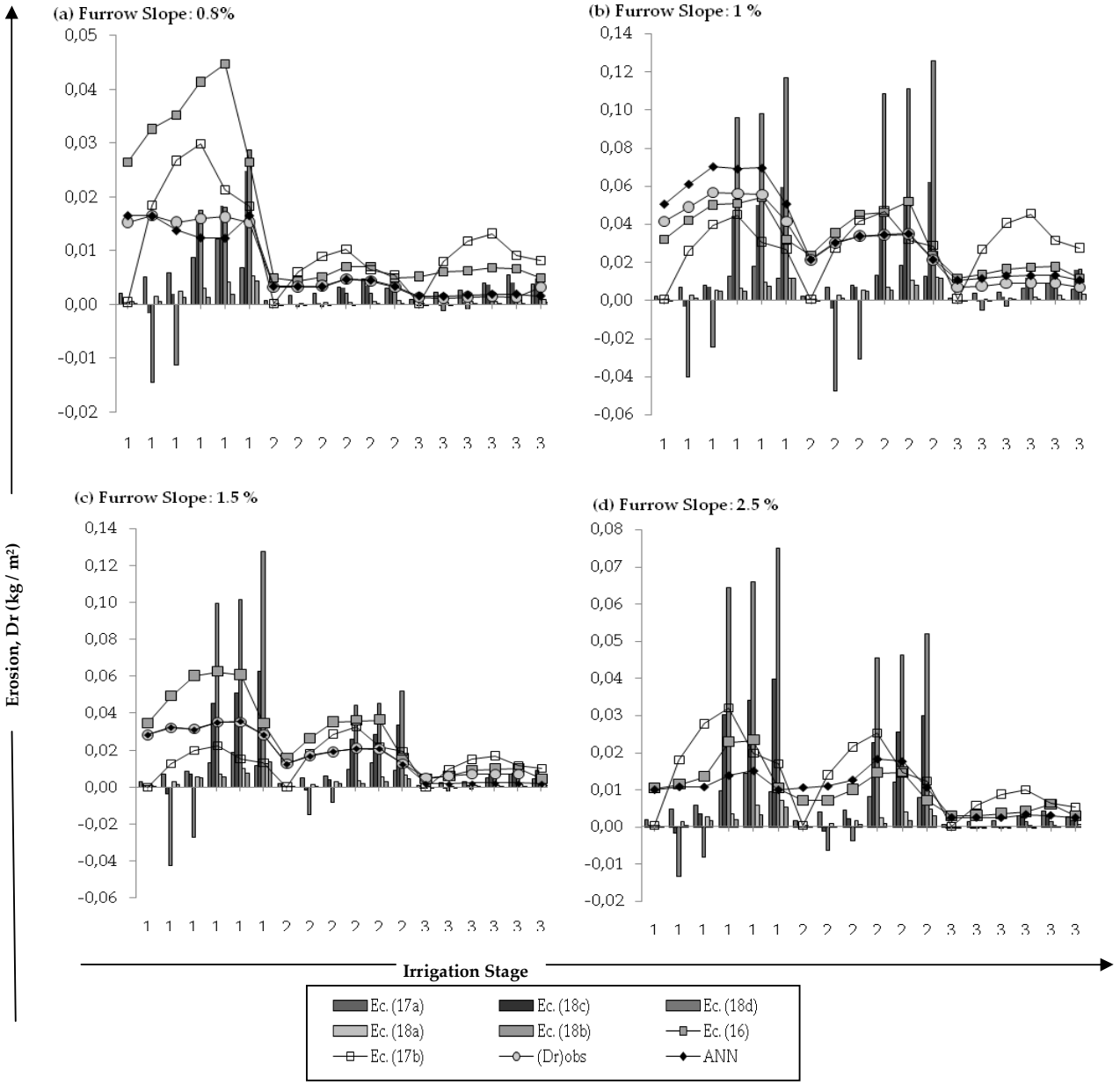

Fig. 12 Comparison of furrow simulated erosion by regression models with observed data.

The cycle under irrigation has been divided into three stages; each stage represents 1/3 of the total duration for 12 weeks, obtaining an averaged data for each phase. In **Fig. 12**, solid lines represent the models by which a satisfactory approximation to the furrow erosion observed data is obtained, and the bars represent the rest of models, where the estimated values differ significantly from the observed data. In general, **Eq. (17b)** achieves the best approximation with respect to the rest of the linear and nonlinear models.

Modeling of furrow erosion based on artificial intelligence techniques

Table 9 shows the fitted statistics to sigmoidal function using the Artificial Neural Network (ANN) technique to

hour and two-hour events, both with different amounts of data. Statistics in the stages of training, validation and testing vary for the networks mentioned before as follows: R^2: For ANN1 in each stage is equal to 0.686; 0.897 and 0.876; for ANN2 in each stage is equal to 0.39; 0.615 and 0.49.

For ANN3 in each stage is equal to 0.758; 0.831 and 0.786. By comparing the errors during the calibration and validation stages, with emphasis on the average absolute error (AAE), the following results are found: AAE varies from 0.1 to 0.14. In general, (a) the error does not vary significantly between stages of calibration, validation and testing, (b) the error tends to be lower as the variability in the data is lower, which promotes a better network learning with respect to the observations made.

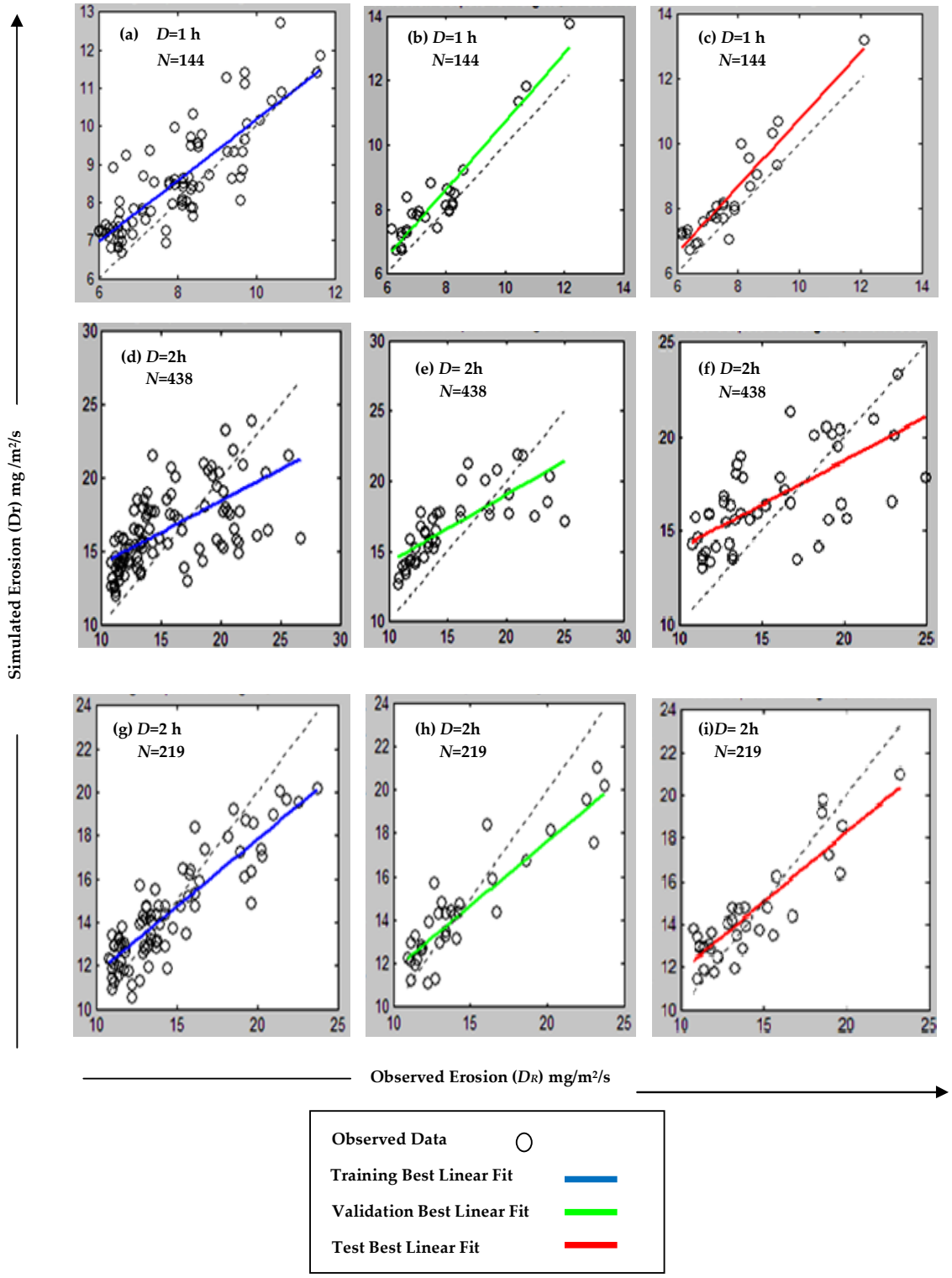

Fig. 13 Comparison of simulated erosion by Artificial Neural Network with observed 1 h and 2h rainfall events.

Comparison of estimated values by the application of ANN's, to the observed data of furrow erosion under rainfall and irrigation events of one and two hours, during the stages of training or calibration, validation and testing, is shown in **Fig. 13**. Vertical axis represents the simulated erosion (D_R sim), and the horizontal axis represents the erosion observed (D_R obs.). Each pair of coordinates is represented by a dot.

Lines in **Figs 13(a)–(i)** represent the ratio of 1:1, where the approximation of points to the lines is a measure of how well the correlation between the set of erosion estimated values using the ANN technique, and

the obtained values by field tests in furrows in different slopes is. **Figures 13a–13c** and **Figs 13g–13i** show the approximate points randomly around the 1:1 line, indicating that the network has successfully learned the pattern shown by observations during rainfall events. **Figures 13d–13f** show that there is a fairly satisfactory approximation of the points to the 1:1 line, which explains that there is some variability in the observations that the network was not able to simulate.

Fuzzy Logic

Modeling furrow erosion using a Fuzzy Inference System

Table 10 shows the two membership functions coefficients for the two input variables to each Fuzzy Inference System (FIS). Characterized FIS's are three: FIS 1 corresponds to natural rainfall events that last an hour, FIS 2 corresponds to the natural rainfall events that last two hours, and FIS 3 corresponds to irrigation events that last two hours. Input 1 is represented by measurements of natural and simulated rainfall (irrigation) in those events that last an hour every 10 minutes, and two hours every 20 minutes. Input 2 is represented by the infiltration values range as shown in **Fig. 7**.

As an example, FIS 1 is described, represented by input membership functions of trapezoidal type. The trapezoidal functions for the rainfall representation have the following parameters: trapmf1: 1.827; 2.974; 4.557 and 5.928. Trapmf2: 4.677; 5.705; 7.562 and 8.709. The trapezoidal functions for the infiltration representation have the following parameters: trapmf1: –0.508; 0.0293, 0.859; 1.381. Trapmf2: 3.637; 4.676; 7.46 and 9.147. The linear output surface has the following parameters: 2.081 for the rainfall; –2.675 for infiltration and 0.0487 for the constant term. The rest of FIS's can be seen in **Table 10**. **Table 11** shows the fitted statistics of erosion modeling under rainfall and irrigation events through the various FIS's from all the observations obtained in field testing in furrows of different slopes. By comparing the Average Absolute Errors during the calibration, validation and testing stages, the following results are found: FIS 1: 1.108; 1.5147 and 1.489; FIS 2: 2.403; 2.5977 and 2.676; FIS 3: 1.4; 2.396 and 1.565, respectively. In general, errors do not vary significantly between the stages of the calibration, validation and testing.

Table 9. Performance criteria of erosion model based on ANN

Model	*N*	*D*	AAE	R^2
(a) During calibration/training				
ANN 1: 6-20-6	144	1	0.13962	0.686
ANN 2: 6-100-6	438	2	0.1750	0.390
ANN 3: 6-100-6	219	2	0.1283	0.758
(b) During validation				
ANN 1: 6-20-6	144	1	0.146	0.897
ANN 2: 6-100-6	438	2	0.166	0.615
ANN 3: 6-100-6	219	2	0.103	0.831
(c) During testing				
ANN 1: 6-20-6	144	1	0.146	0.876
ANN 2: 6-100-6	438	2	0.166	0.490
ANN 3: 6-100-6	219	2	0.1039	0.786

N: number of observed data; *D*: irrigation and rainfall events duration; AAE: average absolute error; R^2: determination coefficient; ANN: artificial neural network

Table 10. Coefficients of membership function from various FIS

Model	Inputs	Membership Function	Parameter- 1	Parameter- 2	Parameter- 3	Parameter- 4
FIS 1	Input 1	Trapmf-1	1.827	2.974	4.557	5.928
	Input 1	Trapmf-2	4.677	5.705	7.562	8.709
	Input 2	Trapmf-1	–0.508	0.0293	0.859	1.381
	Input 2	Trapmf-2	3.637	4.676	7.460	9.147
	Output	linear	2.801	–2.675	0.048	
FIS 2	Input 1	Trapmf-1	–0.9727	0.7139	3.089	5.373
	Input 1	Trapmf-2	3.637	4.676	7.46	9.147
	Input 2	Trapmf-1	–0.5081	0.0293	0.859	1.381
	Input 2	Trapmf-2	3.637	4.676	7.46	9.147
	Output	Linear	5.13	0.1209	–0.179	
FIS 3	Input 1	Trapmf-1	–5.071	–1.601	4.226	7.563
	Input 1	Trapmf-2	5.466	7.789	12.28	15.75
	Input 2	Trapmf-1	–0.501	0.021	0.859	1.381
	Input 2	Trapmf-2	0.979	1.398	2.179	2.717

Table 11. Performance criteria of erosion model based on FIS

Model	*N*	*D*	AAE
(a) During calibration/training			
FIS 1 (trapmf)	88	1	1.108
FIS 2 (trapmf)	262	2	2.007
FIS 3 (trapmf)	180	2	1.400
(b) During validation			
FIS 1 (trapmf)	28	1	1.5147
FIS 2 (trapmf)	88	2	2.1407
FIS 3 (trapmf)	60	2	2.396
(c) During testing			
FIS 1 (trapmf)	28	1	1.489
FIS 2 (trapmf)	88	2	2.367
FIS 3 (trapmf)	60	2	1.565

N: number of observed data; *D*: irrigation and rainfall events duration; AAE: average absolute error; R^2: determination coefficient; ANN: artificial neural network

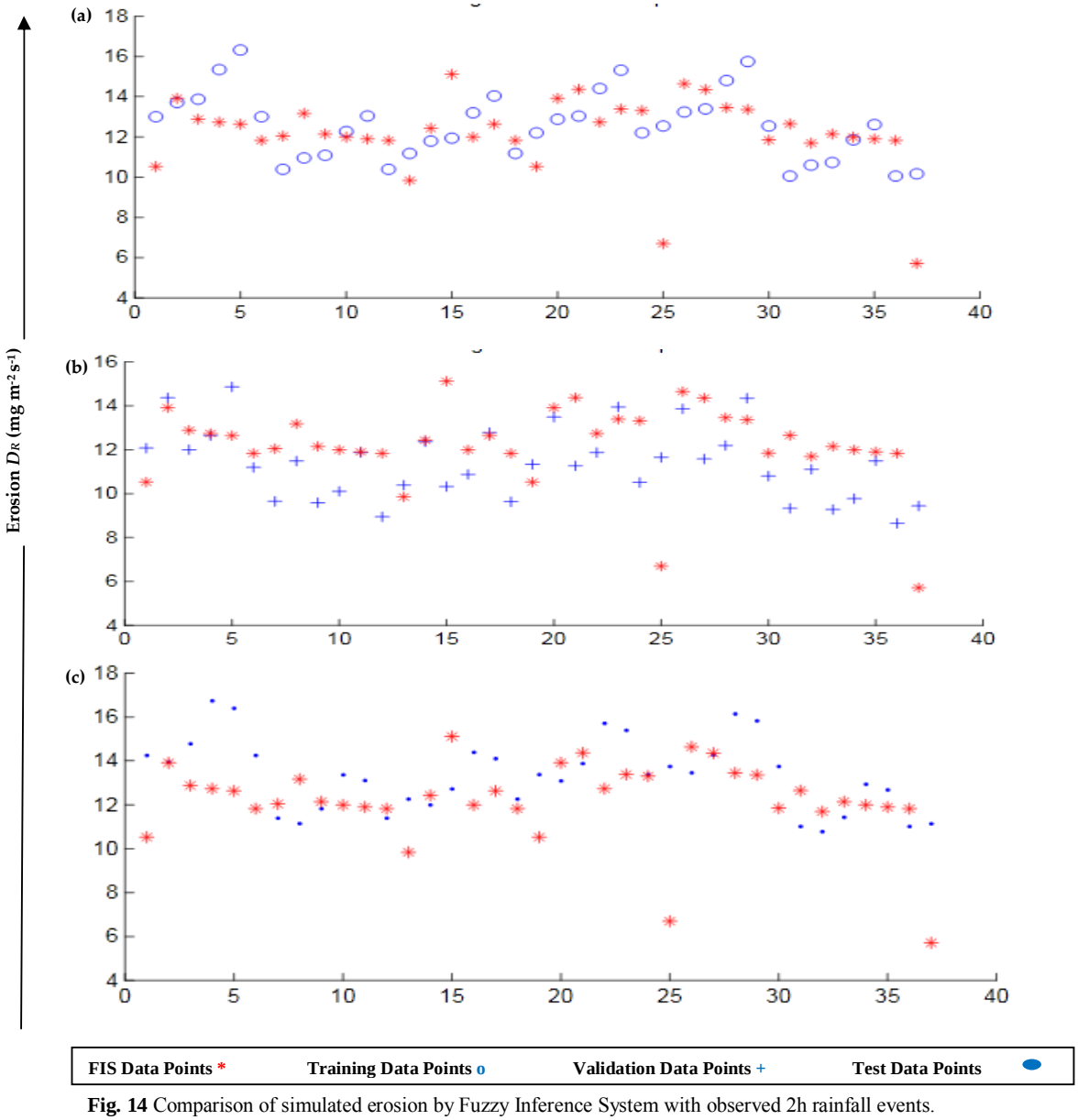

Fig. 14 Comparison of simulated erosion by Fuzzy Inference System with observed 2h rainfall events.

A comparative example of the estimated values by applying the FIS to the observed data of furrow erosion under rainfall events that last two hours, during the stages of training, validation and testing; using a sample of 35 data, is shown in **Fig. 14**. Total number of data in each stage can be seen in **Table 11**. Vertical axis represents the simulated erosion (D_R sim) and the observed (D_R obs). The horizontal axis represents a number assigned to each value; each pair of coordinates is represented by a dot. **Figure 14(a)** shows the results in the training stage of the FIS, which shows that the data points (circles) were satisfactorily approximate to the FIS (asterisks). **Figures 14(b)**–**(c)** show a good approximation of the points found in the FIS.

DISCUSSION OF RESULTS

Comparison of furrow erosion processes simulated with experimental data

Process of particles detachment As shown in the results section, the range of values of concentrated flow erodibility K_c and critical shear stress τ_c, obtained from the fit of the **Eq. (5)** varied between 1.31E–06 and 1.525E–06 s/m, 0.704 and 1.489 Pa, respectively. Knapen *et al.* (2007) conducted a literature review to compile the values of K_c and τ_c reported for different soils and tillage conditions. Studies included: (a) concentrated flow experiments on field plots, and (b) flume experiments in the laboratory. Characteristics of the experimental methods used are summarized in **Tables 12** and **13**. Values ranges have been determined empirically for K_c and τ_c parameters from the excess shear stress linear equation **(Eq. 5)**, including the size of the sample by using field and laboratory experiments, they varied as follows: 0.000 001 and 0.1 m/s (n = 151), 0.01 and 20 Pa (n = 161), 0.00 001 and 0.7 s/m (n = 185), 0.03 and 60 Pa (n = 220), respectively. By comparing these value ranges with those reported on **Table 3** for **Eq. (5),** it was found: (a) K_c values fell within the range for the field experiments and were lower than those found from laboratory experiments, (b) τ_c values were totally included within the reported ranges for the field and laboratory experiments.

From the above, comparisons show that the K_c value range obtained in this study was significantly different from the one reported by Knapen *et al.* (2007), while a lower variation for τ_c value range was found. There are several reasons for these differences, two of the main are (1) differences in experimental conditions in which the data were collected, and (2) the variation of soil types and environmental conditions. By comparing the experimental and environmental conditions of the research described in the methods section with outlined in **Tables 12** and **13**, some similarities were found alike as those in field studies conducted by Bjorneberg *et al.* (1999). With regard to laboratory experiments, cases with which to make a comparison were not found.

The value ranges found for K_c and τ_c by Bjorneberg *et al.* (1999) varied as follows: from 0.0003 to 0.006 m/s and from 1.2 to 1.8 Pa, respectively. Despite the similarities in the experimental conditions shown in **Table 12**, the value range of K_c was significantly different. Causes of the differences appear to be due to environmental conditions, mainly in both climate and agricultural practices, because the experiments of Bjorneberg *et al.* (1999) were made in beans and corn fields, where the wetting and drying sequences, consolidation and residues could be contributing factors to variability of K_c and τ_c values.

In general, the **Eq. (5**) statistics show a satisfactory fit between most of the equation and the observed data, for the following reasons: (1) coefficient of determination R^2 was estimated at 0.7 (Ramírez *et al.*, 2004), (2) Durbin-Watson coefficient presented evidence that there is a slight randomness within consecutive residues, (3) Average Absolute Relative Error and Average Relative Error were moderately low.

Process of sediment transport The ranges of the parameters K_t and b reported in the results section for models of sediment transport capacity represented by **Eqs 7**, **13** and **15** varied as follows: 9.929E–08 and 1.52 669E–07; 7.634 and 34.583; 0.4212 and 0.892, respectively. The value ranges reported for field tests by Finkner *et al.* (1989) and Trout (1999) for **Eq. (7) (Table 14)**, differ significantly from those indicated in **Table 5.** As for **Eq. (13)**, the ω_c critical unit current power value was negative and slightly different from zero, which differs from that proposed by Yang, (1973), which is equal to 0.002 m/s.

Despite the differences, it can be observed that in both cases ω_c tended to zero. According to theory, the ω_c value should be positive. The results of negative ω_c and its low standard error, along with the high correlation make it difficult to explain the physical meaning of the estimated parameter. However, the estimated negative value range of ω_c was not significantly different from zero.

Table 12. Characteristics of field plot in which concentrated flow erosion was measured

Country	Soil (No.)	Slope (%)	Q_{inflow} (l min^{-1})	$I_{rainfall}$ (mm/h)	τ (Pa)	Rill plot dim. (m × m)	Surface Condition	Source
Iran	1	n.a.	132–1693	n.a.	2.2–13.2	15 × 0.3	*I*, varying vegetation cover	Adelpour *et al.* (2004)
USA	1	0.5–1.33	30–40	n.a.	n.a.	Length.:110–256	*I*, residue removed and tilled	Bjorneberg *et al.* (1999)
Brazil	1	n.a.	n.a.	n.a.	n.a.	9 × 0.5	*I*, residue removed and tilled	Braida & Cassol (1996)
Brazil	1	6.7	0–50	74	n.a.	n.a.	n.a.	Cantalice *et al.* (2005)
USA	2	3–15	96–768	n.d.	4.0–37.3	10 × 0.75	*I*, residue removed and tilled	Franti *et al.* (1985; 1999)
Brazil	1	n.a.	0	60	n.a.	9 × 0.5	*I*, residue removed and tilled	Giasson & Cassol, (1996)
USA	30	4–13	7–35	62	n.a.	9 × 0.46	*I*, residue removed and tilled	Gilley *et al.* (1993)
USA	4	0.5–3	n.a.	n.a.	1–36	30.5×0.91	*I*, no cover	Hanson (1989;1990a; 1990b)
USA	1	1–3	4–17.10	n.a.	12–55	29×1.8	*I*, no cover	Hanson & Cook (1999)
USA	2	5–11	n.d.	n.a.	n.a.	10.7×3	*I*, varing canopy cover	Hussein & Laflen (1982)
USA	2	4	11–189	64	0.7–14	4×0.2	*I*, varying tillage practices	King *et al.* (1995)
USA	2	3–15	n.a.	n.a.	n.a.	n.a.	n.a.	Laflen (1987)
USA	56	2–13	0.1–0.6	63	0–22	9–11×0.5–3	*I*, residue removed and tilled	Laflen *et al.* (1991), Elliot *et al.* (1989)
USA	1	3–6	8–38	n.a.	2–10	5.5×2	*I*, residue removed and tilled	Mamo & Bubenzer (2001b)
Canada	3	12–14	n.a.	25–30	n.a.	10×0.8	*I*, vegetation free, seedbed conditions	Merz & Bryan (1993)
USA	1	4–6	8–38	51	1.3–6.1	68.6×6.1	*I*, tilled and all residue buried	Morrison *et al.* (1994)
USA	2	3–5	8–53	64	0–6	6.1×0.76	*I*, residue removed and tilled	Norton & Brown, (1992)
USA	1	27	16–23	n.a.	24–192	6×0.3	*I*, vegetation clipped to various heights	Prosser *et al.* (1995)
Australia	1	1–12.7	1.7–8	n.a.	n.a.	20×1	*I*, vegetation clipped to various heights	Prosser (1996)
Brazil	1	10	12–120	65	2.5–19	6×0.2	n.a.	Reichert *et al.* (2001)
USA	1	2–31	8–60	60	2–7	4.6×0.3	*I*, residue removed and plants clipped	West *et al.* (1992)
USA	1	0.52–1.33	15–46	n.a.	n.a.	204–256	*I*, residue removed and tilled	Trout *et al.* (1999)

n.a.: not available. Soils: number of soil types tested. Slope: slope of soil surface. Q_{inflow}: simulated concentrated flow discharge. $I_{rainfall}$: simulated rainfall intensities. τ: Range of applied flow shear stresses. Rill plot dimensions: length×width. Surface condition: (*S*: smoothened, *I*:irregular)

With respect to **Eq. (15),** comparisons can not be made with the values proposed by Simons *et al.* (1981) because the values reported in literature correspond to flow in rivers.

In general, fitted statistics in **Eqs (7)**, **(13)** and **(15**) indicated a satisfactory approximation between observed and estimated values, for the following reasons: (a) coefficient of determination varied between 0.72 and 0.88, according to Ramirez *et al.* (2004), (b) adjusted R^2 coefficient decreased slightly in relation to R^2, (c) Durbin-Watson coefficient presented evidence that there is a slight randomness between consecutive residues, (3) Average Absolute Relative Error and Average Relative Error were moderately low.

Combination of furrow erosion processes It can be observed from **Figure 11** that the sediment transport capacity values obtained by **Eqs (7**) and **(13)** were lower than the observed sediment load values in the stream for different slopes of furrows in the three stages within the cycle under irrigation, which indicates the occurrence of concentrated flow and deposition process. As for **Eq. (15)**, estimated values of the transport capacity were very close to the sediment load current, therefore, deposition processes occur at low rates. According to theory, the highest proportion of detached sediments is transported out of the furrow (e.g., Nearing *et al.*, 1989, Morgan, 1998; Bulygin *et al.*, 2002).

Table 13. Characteristics of laboratory flume experiments in which concentrated flow erosion was measured

Country	Soil (N°)	Slope (%)	Q_{inflow} (l min^{-1})	$I_{rainfall}$ (mm/h)	τ (Pa)	Flume dim. (m × m × m)	Source	Remark
Italy	6	10–40	2.4–18	/	1–12	1.5 × 0.2	Ciampallini & Torri (1998)	a
Australia	1	2–7	2.5–40	/	n.a.	1.8 × 0.6 × 0.2	Crouch & Novruzi (1989)	b, e
Mexico	1	0	n.a.	/	1.1–38.2	4.9 × 0.3 × 2.5	Ghebreiyessus *et al.* (1994)	
Belgium	2	5–21	3.3–60	/	1–24	4 × 0.4 × 0.45	Giménez & Govers (2002)	
Belgium	2	9–21	6.7–60	/	1–16	2 × 0.10 × 0.09	Giménez & Govers (2002)	
Belgium	2	1.5–7	0.7–10.4	/	0,1–1,3	6 × 0.12	Govers (1985)	b, e
Belgium	1	20–30	18–114	/	4.4–22.4	2 × 0.1 × 0.09	Gyssels *et al.* (2006)	
Canada	5	n.a.	n.a.	/	n.a.	9.1 × 0.15	Kamphuis & Hall (1983)	b, e
USA	5	0.2	n.a.	/	n.a.	18.3 × 0,77 × 0,46	Laflen & Beasley (1960)	a, e
USA	7	0.2	n.a.	/	n.a.	22 × 0.4 × 0.76	Lyle & Smerdon (1965)	a, e
USA	1	3–5	7.6–37.9	/	n.a.	4 × 0.2 × 0.05	Mamo & Bubenzer (2001a)	
Canada	1	14	/	34	n.a.	10 × 0.8 × 0,2	Merz & Bryan (1993)	b, c, e
USA	8	n.a.	6.1–30.3	/	0–3.2	1.84 × 0.1 × 0,19	Moody *et al.* (2005)	e
Belgium	1	10–35	5.6–11.5	/	1.6–5.7	2 × 0.1 × 0.09	Nachtergaele & Poesen (2002)	
USA	1	n.a.	n.a.	/	0.1–1.3	18.3 × 0.3 × 0.38	Partheniades (1965)	e
S-Africa	12	2–20	0.08–0.32	/	0,2–4.9	0.5 × 0.05 × 0.13	Rapp (1998)	
Israel	3	2–20	0.08–0.32	/	0.2–4.9	0.5 × 0.05 × 0.13	Rapp (1998)	
Belgium	1	2.6–14	n.a.	/	n.a.	2 × 0.4	Rauws (1987)	
Belgium	1	3–33	n.a.	20	n.a.	2.5 × 0.6	Rauws & Govers (1988)	b, c, e
USA	1	2–20	0.04–0.2	/	0.4–4.8	0.5 × 0.05 × 0.12	Shainberg *et al.* (1994)	b, e
Israel	3	5	0.04–0.32	/	0.8–1.8	0.5 × 0.05 × 0.12	Shainberg *et al.* (1996)	
Australia	16	5–30	0.1–1.8	100	n.a.	3 × 0.8 × 0.15	Sheridan *et al.* (2000a,b)	d
Canada	1	9	n.a.	35	n.a.	15 m long.	Slattery & Bryan (1992)	
USA	11	0–1	n.a.	/	n.a.	18.3 × 0.77 × 0.46	Smerdon & Beasley (1959)	
USA	5	0.1–0.2	n.a.	0–127	n.a.	22 × 0.8	Smerdon (1964)	
Italy	4	1–31	n.a.	15–110	0–3.3	2 × 0.5 × 0.1	Torri *et al.* (1987)	
USA	1	7	2–4	/	1.9–3.9	2.73 × 0.46 × 0.88	Van Klavern & McCool (1998	
China	1	10,5–21.2	2.5–6.5	/	1–10	5 × 0.3	Zhang *et al.* (2005)	a
USA	5	1.5–5	3.8–15.1	/	0.5–2.5	6.4 × 0.15 × 0.05	Zhu *et al.* (1995)	
USA	5	0–5.5	n.a.	/	0.5–2.5	6.4 × 0.15 × 0.05	Zhu *et al.* (2001)	

n.a.: not available. /:not applicable. Soils: number of soil types tested. Slope: slope of soil surface. Q_{inflow}: simulated concentrated flow discharge. $I_{rainfall}$: simulated rainfall intensities. τ: Range of applied flow shear stresses. Flume dimensions: length×width×depth. Remarks: (a) values for K_c and/or τ_c deduced from graphs, (b) values calculated from critical shear velocity, (c) values for poorly cohesive or non-cohesive soils, (d) tests on coal mine soils and overburdens, (e) excess shear stress equation was not used to deduce K_c and/or τ_c.

Table 14. Models parameters to estimate sediment transport capacity of flow in furrow and characteristics of field tests

$T_c = K_t(\tau)^b$										
Source	T_c (kg/m/s)	K_t	τ(Pa)	b	Slope (%)	Q (L / min)	$I_{rainfall}$ (mm/ h)	Rill plot dim. (m×m)	Surface condition	Remark
Finkner *et al.* (1989)	0.0006–0.2366	0,015–0,05	1–6	1.5	2–20	n.a.	80–83	10, 50, 100 m long	n.a.	b
Trout (1999)	0.002–0.035	0,017–0,065	n.a.	2	1.3	6–18	n.a.	204 m long	residue removed and tilled	a
	0.001–0.02	0,015–0,15	n.a.	4	0.5	6–45.6	n.a.	256 m long	residue removed and tilled	a
$T_c = c[(\omega-\omega_c)/V_s]^b$										
Source	T_c (ppm)	C	ω_c (m/s)	b	Slope (%)	Q_{inflow} (L/min)	$I_{rainfall}$ (mm/h)	Rill plot dim. (m×m)	Surface condition	Remark
Loch (1984)	41.000–87.000	n.a.	0.002	n.a.	4	15–107	95	0.4×1.5–22.5	removed and tilled	b

n.a.: not available. Remark: K_t: (a) obtained by empirical fit, (b) obtained by equation of Yalin (1963).

Trout (1996) found that at the end of the furrows of bean crops, erosion increases from the beginning to the end of the cycle from 1 to 5 Mg/ha, while the process was reversed in the corn crop due to the reduction of erosion from 2 to 0.1 Mg/ha at the end of the cycle. In furrows was not significant, based on the uniformity of both water supplies through the sprinklers as well as frequency of wetting in each furrow. The erosion rate, from the beginning to the end of the cycle, varied from 0.6 to 0.1 Mg/ha (**Fig. 12**). This range is lower than that

Trout (1999) reported sediment transport rates in furrows of slope at 1.3% and 5.2% for corn and bean, that varied from the beginning to the end of the cycle as follows: from 20 000 to 4000 $mg \cdot s^{-1}m^{-1}$, from 25 000 to 5000 $mg \cdot s^{-1}m^{-1}$, respectively. These ranges were higher than those found in this study, which varied from 1428 to 10 000 $mg \cdot s^{-1}m^{-1}$ (mg of sediment per meter of wetted perimeter per second).

Furrow erosion models based on regressions Estimated erosion values by the multiple linear models were closer to the field observations than those which were obtained by models based on nonlinear polynomials. Linear model showed that the maximum loads of sediments during events of natural and artificial rain were successfully estimated. However, there was a lack of adjustment for values at the beginning and at the end of such events, which coincides with the results of Jain *et al.* (2004), Kumar (2001) and Srinivasulu *et al.* (2006) (**Fig. 12**). Findings in polynomial-based models indicate that the estimation process of the observed variable tends to decrease as the power increases.

Modeling of furrow erosion using artificial intelligence techniques

Artificial Neural Networks Estimated erosion values by artificial neural networks became successfully closer to the observations during the stages of calibration, validation, and testing, in terms of the coefficient of determination and the Average Absolute Error. The ANN estimate improved as the variability of data for training and testing of the network was lower, which helped the network to learn the pattern of data.

Fuzzy Inference System Estimated erosion values by FIS's became successfully closer to the observations during the stages of calibration, validation and testing, in terms of the Average Absolute Error. The pattern in the input data was better represented by using the trapezoidal function both for rainfall, as well as for infiltration. The system output was represented by a multiple linear equation. Estimated erosion resulted closer to observations in the stages of training, validation and testing (**Fig. 14).** Estimation by ANN improved as the variability of data for training and testing of the network was lower, which helped the network to learn the pattern of data. The application of FIS's has been used successfully for modeling of reservoir operation by Panigrahi (2000), which validates its use for simulating hydrological processes.

Comparison of models to estimate rill erosion The differences between the dynamic versions of the WEPP and EUROSEM models were significant in the magnitudes of the events; however, both of them estimated the erosion processes, namely, sediment model was different from WEPP and EUROSEM models because they produced smaller estimates of deposition process.

The comparison between the different models indicates the following order on the quality of the estimation in furrow erosion: Artificial intelligence techniques, models based on physical processes, linear regression, and finally, the non-linear regression **(Fig. 12)**.

CONCLUSIONS

It is possible to make estimates of the physical processes of erosion in furrows with a moderate to high accuracy, although it is believed that the estimation can be increased and improved by making adjustments of the models for each slope of furrow.

Models based on linear regressions achieved better estimates at the observed values than the nonlinear models based on polynomials. This should be emphasized in training with new data to better estimate the values at the beginning and end of natural and artificial rain events.

Modeling of furrow erosion using artificial intelligence techniques resulted in a satisfactory approximation of the estimated values to those observed, improving accuracy through the application of ANN's with respect to the FIS's. The estimation quality improves as variability in the model data is low.

The comparison between the different models indicate the following order on the quality of the estimation of furrow erosion: artificial intelligence techniques, models based on physical processes, linear regression and finally, the non-linear regression

Acknowledgment The research was developed in *Centro de Investigaciones Hidrológicas y Ambientales de la Universidad de Carabobo* (CIHAM-UC) with the financial support of CDCH-UC and FONACIT.

REFERENCES

AMERICAN PUBLIC HEALTH ASSOCIATION (1995) Standard Methods for The Examination of Water and Wastewater. American Public Health Association, United States of America, Washington, DC, 19th Edition. 2–53.

AMERICAN SOCIETY FOR TESTING AND MATERIALS (2007) *Standard Test Methods for particle-size analysis of soils*. American Society for Testing and Materials International, United States of America, West Conshohocken. (Reaproved 2007), 1–8.

Adelpour, A.A., Soufi, M. & Behnia, A.K. (2004) Channel erosion thresholds for different land uses assessed by concentrated overland flow on a silty loam. *Proc. International Soil Conservation Organisation Conference.* Brisbane, Australia.

Alonso C.V., Neibling, W.H. & Foster, G.R. (1981) Estimating sediment transport capacity in watershed modeling. *Trans. ASAE* **24**(5), 1211–1220.

Bjorneberg, D.L., Trout, R.E., Sojka, R.E. & Aase, J.K. (1999) Evaluating WEPP predicted infiltration, runoff and soil erosion

Braida, J.A. & Cassol, E.A. (1996) Rill and interrill erodibility of a paleudult soil. *Rev. Bras. Ciênc. Solo* **20**(1), 127–134.

Bulygina, N.S., Nearing, M.A., Stone, J.J. & Nichols, M.H. (2007) DWEPP: a dynamic soil erosion model based on WEPP source terms. *Earth Surf. Processes Landf.* **32**(7), 998–1012. doi: 10.1002/esp.1467.

Bulygin, S.Y., Nearing, M.A. & Achasov, A.B. (2002) Parameters of interrill erodibility in the WEPP model. *Eurasian Soil Sci.* **35**(11), 1237–1242.

Bishop, C.M. (1994) Neural networks and their applications. *Rev. Sci.Instrum.* **65**(6), 1803–1832.

Cantalice, J.R.B., Cassol, E.A., Reichert, J.M. & Borges, A.L.D. (2005) Flow hydraulics and sediment transport in rills of a sandy clay loam soil. *Rev. Bras. Ciênc. Solo* **29**(4), 597–607. (in portuguese). doi: 10.1590/S0100-06832005000400012.

Ciampallini, R. & Torri, D. (1998) Detachment of soil particles by shallow flow: sampling methodology and observations. *Catena* **32**(1), 37–53. doi:10.1016/S0341-8162(97)00050-7.

Crouch, R.J. & Novruzi, T. (1989) Threshold conditions for rill initiation on a vertisol, Gunnedah, N.S.W., Australia. *Catena* **16**(1), 101–110. doi:10.1016/0341-8162(89)90007-6.

Demuth, H., Beale, M., Hagan, M. (2009) *Neural Network Toolbox*. User Guide. MATLAB.

Elliot, W.J., Liebenow, A.M., Laflen, J.M. & Kohl, K.D. (1989) *A compendium of soil erodibility data from WEPP cropland soil field erodibility experiments 1987–1988*. NSERL Rpt. No. 3. Ohio State University and Natural Soil Erosion Research Laboratory, Agricultural Research Service, U.S. Department of Agriculture, W. Lafayette, Indiana.

Flanagan, D.C., Ascough, J.C., Nearing, M.A. & Laflen, J.M. (2001) *The Water Erosion Prediction Project model*. In: Harmon, R.S. & Doe, W.W. (eds) Landscape Erosion and Evolution Modelling, Kluwer: New York, 145–199.

Flanagan, D.C. & Nearing, M.A. eds. (1995) USDA–Water Erosion Prediction Project (WEPP), Hillslope Profile and Watershed Model Documentation Technical Documentation, NSERL Report 10. USDA-ARS National Soil Erosion Research Laboratory: West Lafayette, IN.

Finkner, S.C., Nearing M.A., Foster G.R. & Gilley J.E. (1989) A simplified equation for modeling sediment transport capacity. *Trans. ASAE* **32**(5), 1545–1550.

Foster, G.R. & Meyer, L.D. (1972) Transport of particles by shallow flow. *Trans. ASAE* **15**(1), 99–102.

Foster, G.R. & Meyer, L.D. (1975) Mathematical simulation of upland erosion using fundamental erosion mechanics. *Proc. Sediment Yield Workshop*. U.S. Sedimentation Laboratory, Oxford, MI, 190–201.

Foster, G.R. (1982) *Modeling the erosion process*. In: Hahn, C.T. (Ed.). Hydrologic Modeling of Small Watersheds, 295–380.

Foster, G.R., Huggins, L.F. & Meyer, L.D. (1984) A laboratory study of rill hydraulics: shear stress relationships. *Trans. ASAE* **27**(3), 797–804.

Foster, G.R. & Lane, L.J. (1987) *User Requirements: USDA-WEPP* (Draft 6.3) National Soil Erosion Research Laboratory, West Lafayette, Indiana.

Foster, G.R. (1990) *Major developments in prediction of soil erosion by water*. In: Lal, R. & Pierce, F.J. (eds.) Soil Management for Sustainability Soil and Water Conservation Society, Ames, Iowa.

Franti, F.G., Laflen, J.M. & Watson, D.A. (1985) *Soil erodibility and critical shear under concentrated flow*. ASAE Paper No. 85-2033

Franti, T.G., Laflen, J.M. & Watson, D.A. (1999) Predicting soil detachment from high discharge concentrated flow. *Trans. ASAE* **42**(2), 329–335.

Ghebreiyessus, Y.T., Gantzer, C.J., Alberts, E.E. & Lentz, R. (1994) Soil erosion by concentrated flow: shear stress and bulk density. *Trans. ASAE* **37**(6), 1791–1797.

Giménez, R. & Govers, G. (2002) Flow detachment by concentrated flow on smooth and irregular beds. *Soil Sci. Soc. Am. J.* **66**(5), 1475–1483. doi:10.2136/sssaj2002.1475.

Gyssels, G., Poesen, J., Van Dessel, W., Knapen, A. & Debaets, S. (2006) Effects of cereal roots on detachment rates of single and doubledrilled topsoils during concentrated flow. *Eur. J. Soil Sci.* **57**(3), 381–391. doi: 10.1111/j.1365-2389.2005.00749.x.

Giasson, E. & Cassol, E.A. (1996) Rill erosion related to inflow rates and amounts of incorporated wheat straw in a sandy clay loam Paleudult soil. *Rev. Bras. Ciênc. Solo* **20**(1), 117–125.

Gilley, J.E., Elliot, W.J., Laflen, J.M. & Simanton, S.R. (1993) Critical shear stress and critical flow rates for initiation of rilling. *J. Hydrol.* **142**(2), 251–271. doi:10.1016/0022-1694(93)90013-Y.

Govers, G. (1985) Selectivity and transport capacity of thin flow in relation to rill erosion. *Catena* **12**(1), 35–49. doi:10.1016/S0341-8162(85)80003-5.

Guevara, E. & Márquez, A. (2009) Modelación de la erosión y transporte de sedimentos en un campo agrícola bajo riego. *Tecnología y Ciencias del Agua* (Submitted).

Hanson, G.J. (1989) *An in-situ erodibility testing device*. American Society of Agricultural Engineers - Canadian Society of Agricultural Engineers. Paper No. 89–2151.

Hanson, G.J. (1990a) Surface erodibility of earthen channels at high stresses. Part II-Developing an in situ testing device. *Trans. ASAE* **33**(1), 132–137.

Hanson, G.J. (1990b) Surface erodibility of earthen channels at high stresses part I. Open channel testing. *Trans. ASAE* **33**(1), 127–131.

Hanson, G.J., Cook, K.R. & Simon, A. (1999) Determinig erosion resistance of cohesive materials. American Society of Civil Engineers, *Proc. International Water Resources Engineering Conference*. Seattle, Washington, USA.

Hussein, M.H. & Laflen, J.M. (1982) Effects of crop canopy and residue on rill and interrill soil erosion. *Trans. ASAE* **25**(5), 1310–1315.

Jain, A. & Ormsbee, L.E. (2002) Evaluation of short-term water demand forecast modeling techniques: conventional methods versus AI. *J. American Water Works Assoc.* **94**(7), 64–72.

Jain, A., Sudheer, K.P. & Srinivasulu, S. (2004) Identification of physical processes inherent in artificial neural network rainfall runoff models. *Hydrol. Processes* **118**(3), 571–581. doi: 10.1002/hyp.5502.

Juarez, E. & Rico, A. (1991) *Mecánica de Suelos*. Ed. Limusa. Mexico.

Kamphuis, J.W. & Hall, K.R. (1983) Cohesive material erosion by unidirectional current. J. Hydr. Engrg. **110**(3), 370–370. doi: 10.1061/(ASCE)0733-9429(1984)110:3(370).

Knapen, A., Poesen, J., Govers, G., Gyssels, G. & Nachtergaele, J. (2007) Resistance of soils to concentrated flow erosion: A review. *Earth-Science Rev.* **80**(2), 75–109. doi:10.1016/j.earscirev.2006.08.001.

King, K.W., Flanagan, D.C., Norton, L.D. & Laflen, J.M. (1995) Rill erodibility parameters influenced by long-term management practices. *Trans. ASAE* **38**(1), 159–164.

Koluvek, P.K., Tanji, K.K. & Trout, T.J. (1993) Overview of soil erosion from irrigation. *J. Irrig. Drainage Engr. ASCE* **119**(6), 929–946. doi: 10.1061/(ASCE)0733-9437(1993)119:6(929).

Klik, A., Savabi, M.R., Norton, L.D. & Baumer, O. (1995) Application of WEPP hillslope model on Austria. *Proc. Annual Conference of the American Water Resources Association* (AWRA). Houston, Texas, 313–322.

Kumar, A. & Minocha, K. (2001) Rainfall runoff modeling using artificial neural networks. *J. Hydrol. Eng.* **6**(2), 176–177. doi: 10.1061/(ASCE)1084-0699(2001)6:2(176).

Laflen, J.M. & Beasley, R.P. (1960) *Effects of compaction on critical tractive forces in cohesive soils*. University of Missouri. Experiment Station Research Bulletin, **749**.

Laflen, J.M. (1987) *Effect of tillage systems on concentrated flow*

Proc. 40 International Conference on Soil Conservation, Maracay, República Bolivariana de Venezuela.

Laflen, J.M., Elliot, W.J., Simanton, J.R., Holzhey, C.S. & Kohl, K.D. (1991) WEPP: Soil erodibility experiments for rangeland and cropland soils. *J. Soil Water Conserv.* **46**(1), 39–44. doi: 10.2489/jswc.46.1.39.

Laflen, J.M., Flanagan, D.C. & Engel, B.A. (2004) Soil erosion and sediment yield prediction accuracy using WEPP. *J. Am. Water Res. Assoc.* **40**(2), 289–297. doi: 10.1111/j.1752-1688.2004.tb01029.x.

Lyle, W.M. & Smerdon, E.T. (1965) Relation of compaction and other soil properties to erosion resistance of soils. *Trans. ASAE* **8**(4), 419–422.

Loch, R.J. (1984) Field rainfall simulator studies on two caly spils of the Darling Downs, Queensland, III, An evaluation of currents methods of deriving soil erodibilities (K factors), *Aust. J. Soil Res*. **22**(4), 401–412.

Mamo, M. & Bubenzer, G.D. (2001a) Detachment rate, soil erodibility and soil strength as influenced by living plant roots part I: laboratory study. *Trans. ASAE* **44**(5), 1167–1174.

Mamo, M. & Bubenzer, G.D. (2001b) Detachment rate, soil erodibility and soil strength as influenced by living plant roots part II: field study. *Trans. ASAE* **44**(5), 1175–1181.

MATLAB. (2010) *Fuzzy Logic Toolbox*. User's Guide. The Mathworks Inc.

Merz, W. & Bryan, R.B. (1993) Critical threshold conditions for rill initiation on sandy loam Brunisols: laboratory and field experiments in southern Ontario, Canada. *Geoderma* **57**(4), 357–385. doi: 10.1016/0016-7061(93)90050-U.

Meyer-Peter, E. & Müller R. (1948) Formulas for bed-load transport. Proc. II Meeting IARH, Stockholm, 39–64.

Moody, J.A., Smith, J.D. & Ragan, B.W. (2005) Critical shear stress for erosion of cohesive soils subjected to temperatures typical of wildfire. *J. Geophys. Res.* **110**, F01004. doi: 10.1029/2004JF000141.

Morrison, J.E., Richardson, C.W., Laflen, J.M. & Elliott, W.J. (1994) Rill erosion of a Vertisol with extended time since tillage. *Trans. ASAE* **37**(4), 1187–1196.

Morgan, R.P.C., Quinton, J.N., Smith, R.E., Govers G., Poesen, J.W. A., Auerswald, K., Chisci, G., Torri, D. & Styczen, M.E. (1998) The European Soil Erosion Model (EUROSEM): A dynamic approach for predicting sediment transport from fields and small catchments. *Earth Surf. Processes Landf.* 23(6), 527–544. doi: 10.1002/(SICI)1096-9837(199806)23:6.

Nachtergaele, J. & Poesen, J. (2002) Spatial and temporal variations in resistance of loess-derived soils to ephemeral gully erosion. *European J. Soil Sci.* **53**(3), 449–463. doi: 10.1046/j.1365-2389.2002.00443.x.

Nearing M.A., Foster G.R., Lane L.J. & Finkner S.C. (1989) A process-based soil erosion model for USDA–Water Erosion Prediction Project technology. *Trans. ASAE* **32**(5), 1587–1593.

Nearing, M.A., Bulygin, S.Y. & Kotova, M.M. (1998) Primary verification and adaptation of the WEPP model for Ukrainian conditions: problems, possible solutions, and perspectives. *Pochvovedenie* **31**(2), 96–99.

Norton, L.D. & Brown, L.C., (1992) Time-effect on water erosion for ridge tillage. *Trans. ASAE* **35**(2), 473–478. 1992.

Lambe, T.W. & Whitman, R.V. (1972) Mecanica de Suelos. Ed. Limusa. Mexico.

Panigrahi, D.P. & Mujumdar, P.P. (2000) Reservoir operation modelling with Fuzzy Logic. *Water Res. Manag.* **14**(2) 89–109. doi: 10.1023/A:1008170632582.

Partheniades, E. (1965) Erosion and deposition of cohesive soils. Journal of the Hydraulics Division. Proc. American Society of Civil Engineers, 105–139.

Prosser, I.P., Dietrich, W.E. & Stevenson, J. (1995) Flow resistance and sediment transport by concentrated overland flow in a grassland valley. *Geomorphol.* **13**(1), 73–86. doi:10.1016/0169-

Prosser, I.P. (1996) Thresholds of channel initiation in historical and Holocene times. *Adv. Hills. Processes* **2**(7), 687–708.

Rapp, I. (1988) *Effects of soil properties and experimental conditions on the rill erodibilities of selected soils*. Ph. D. Thesis, Faculty of Biological and Agricultural Sciences, University of Pretoria, South Africa.

Ramirez, H. & De La Vara, R. (2004) *Análisis y diseño de experimentos*. Mc Graw Hill. México.

Rauws, G. (1987) *The initiation of rills on plane beds of non-cohesive sediments*. In: Catena Supplement, **8**, 107–118.

Rauws, G. & Govers, G. (1988) Hydraulic and soil mechanic aspects of rill generation on agricultural soils. *J. Soil Sci.* **39**(2), 111–124.

Ranieri, S.B.L, Sparovek, G., Demaria, I.C. & Flanagan, D.C. (1999) Erosion rate estimation using USLE and WEPP on a Brazilian watershed. *Proc. International Soil Conservation Organization Conference*. West Lafayette, IN.

Renard, K.G., Foster, G.R., Weesies, G.A, McCool D.K. & Yoder, D.C. (1997a) *Predicting Rainfall Erosion Losses: a Guide to Conservation Planning with the Revised Universal Soil Loss Equation (RUSLE)*. USDA Agricultural Handbook 703. US Government Printing Office: Washington, DC.

Renard, K.G., Foster, G.R., Weesies, G.A. & Porter J.P. (1997b) RUSLE – Revised Universal Soil Loss Equation. *J. Soil Water Conserv.* **49**(3), 213–220.

Reichert, J.M., Schäfer, M.J., Cassol, E.A. & Norton, L.D. (2001) *Interrill and rill erosion on a tropical sandy loam soil affected by tillage and consolidation*. In: Stott, D.E., Mohtar, R.H. & Steinhardt, G.C. (eds.), Sustaining the Global Farm. Proc. 10th International Soil Conservation Organization Meeting, May 24–29, 1999, Purdue University and the USDA-ARS Soil Erosion Research Laboratory, USA.

Santoro, V.C., Amore, E., Modica, C. & Nearing, M.A. (2002) Application of two erosion models to a large Sicilian basin. *Proc. Int. Congress of European Soc. for Soil Conservation*, Valencia.

Santos, C.A.G., Srinivasan, V.S., Suzuki, K. & Watanabe, M. (2003) Application of an optimization technique to a physically based erosion model. *Hydrol. Processes* **47**, 989–1003, doi: 10.1002/hyp.1176.

Savabi, M.R., Klik, A., Grulich, K., Mitchell, J.K. & Nearing, M.A. (1996) Application of WEPP and GIS on small watersheds in USA and Austria. *Proc. HydroGIS 96: Application of Geographic Information Systems in Hydrology and Water Resources Management*. IAHS Publication **235**.

Simons, D. B., Li, R.M. & Fullerton, L. (1981) *Theoretically derived sediment transport equations for Pima County, Arizona. Prepared for Pima County DOT and Flood Control District*, Tucson, Arizona, Colorado.

Shainberg, I., Laflen, J.M., Bradford, J.M. & Norton, L.D. (1994) Hydraulic flow and water quality characteristics in rill erosion. *Soil Sci. Soc. Am. J.* **58**(4), 1007–1012. doi: 10.2136/sssaj1994.03615995005800040002x.

Shainberg, I., Goldstein, D. & Levy, G.J. (1996) Rill erosion dependence on soil water content, aging, and temperature. *Soil Sci. Soc. Am. J.* **60**(3), 916–922. doi:10.2136/sssaj1996.03615995006000030034x.

Sheridan, G.J., So, H.B., Loch, R.J., Pocknee, C. & Walker, C.M. (2000a) Use of laboratory-scale rill and interrill erodibility measurements for the prediction of hillslope-scale erosion on rehabilitated coal mine soils and overburdens. *Aust. J. Soil Res.* **38**(2), 285–297. doi:10.1071/SR99039.

Sheridan, G.J., So, H.B., Loch, R.J. & Walker, C.M. (2000b) Estimation of erosion model erodibility parameters from media properties. *Australian J. Soil Res.* **38**(2), 256–284. doi: 10.1071/SR99041.

Silva, R.M., Santos, C.A.G. & Silva, L.P. (2007) Evaluation soil loss in Guaraira basin by GIS and remote sensing based model. *J. Urban and Environ. Eng.* **1**(2), 44–52, doi: 10.4090/juee.2007.v1n2.044052.

Slattery, M.C. & Bryan, R.B. (1992) Hydraulic conditions for rill incision under simulated rainfall: a laboratory experiment. *Earth Surf. Processes Landf.* **17**(1), 127–146. doi: 10.1002/esp.3290170203.

Smerdon, E.T. (1964) Effect of rainfall on critical tractive forces in channels with shallow flow. *Trans. ASAE*, Paper No. 63-700.

Smerdon, E.T. & Beasley, R.P. (1959) *The tractive force theory applied to stability of open channels in cohesive soils*. Agricultural Experiment Station University of Missouri Research Bulletin **715.**

Smith, R. E., Goodrich, D. & Quinton, J. N. (1995) Dynamic distributed simulation of watershed erosion: the KINEROS2 and EUROSEM models. *J. Soil Water Conserv.* **50**(5), 517–520.

Terzaghi, K. & Peck, R.B. (1967) *Soil Mechanics in Engineering Practice*, 2a. ed. John Wiley and Sons, New York.

Torri, D. (1987) A theoretical study of soil detachability. In: Catena Supplement, **10**, 15–20.

Trout, T.J. & Neibling, W.H. (1993) Erosion and sedimentation processes on irrigated fields. *J. Irrig. Drainage Engr. ASCE* **119**(6), 947–963. doi: 10.1061/(ASCE)0733-9437(1993)119:6(947).

Trout. T.J. (1996) Furrow erosion and sedimentation: on field distribution. *Trans. ASAE* **39**(5), 1717–1723. 1996

Trout, T.J. (1999) *Sediment transport in irrigation furrows*. In: Sustaining the Global Farm: Selected Papers from the 10th Intl. Soil Conservation Organization Meeting, 710–716. In: Stott, D.E., Mothar, R.H. & Steinhardt, G.C. (eds.) West Lafayette, Ind.: Purdue University and USDA-ARS National Soil Erosion Research Laboratory.

Van Klaveren, R.W. & MccooL, D.K. (1998) Erodibility and critical shear of a previously frozen soil. *Trans. ASAE* **41**(5), 1315–1321.

West, L.T., Miller, W.P., Bruce, R.R., Langdale, G.W., Laflen, J.M. & Thomas, A.W. (1992) Cropping system and consolidation effects on rill erosion in the Georgia Piedmont. *Soil Sci. Soc. Am. J.* **56**(4), 1238–1243. doi: 10.2136/sssaj1992.03615995005600040038x.

Wischmeier W.H. & Smith D.D. (1958) Rainfall energy and its relationship to soil loss. *Trans. Am. Geophys. Union* **39**(2), 285–291.

Yalin Y.S. (1963) An expression for bed-load transportation. *Journal of Hydraulics Division ASCE* **89**(HY3), 221–250.

Zeleke, G. (1999) Application and adaptation of WEPP to the traditional farming system of the Ethiopian highlands. *Proc. International Soil Conservation Organization Conference*. West Lafayette, Indiana.

Zhang, X.C., Nearing, M.A., Risse, L.M. & McGregor, K.C. (1996) Evaluation of runoff and soil loss predictions using natural runoff plot data. *Trans. ASAE* **39**(3), 855–863.

Zhang, X.C., Li, Z.B. & Ding, W.F. (2005) Validation of WEPP sediment feedback relationships using spatially distributed rill erosion data. *Soil Sci. Soc. Am. J.* **69**(5), 1140–1147. doi:10.2136/sssaj2004.0309.

Zhu, J.C., Gantzer, C.J., Peyton, R.L., Alberts, E.E. & Anderson, S.H. (1995) Simulated small-channel bed scour and head cut erosion rates compared. *Soil Sci. Soc. Am. J.* **59**(1), 211–218. doi:10.2136/sssaj1995.03615995005900010032x.

Zhu, J.C., Gantzer, C.J., Anderson, S.H., Peyton, R.L. & Alberts, E.E. (2001) Comparison of concentrated flow-detachment equations for low shear stress. *Soil Till. Res.* **61**(3), 203–212. doi:10.1016/S0167-1987(01)00207-0.